Development of numerical methods to simulate the melting of a thermal protection system.

S. Peluchon[a,*], G. Gallice[a,**], L. Mieussens[b,c]

[a] *CEA-CESTA, 15 avenue des sablières - CS 60001, 33116 Le Barp Cedex, France*
[b] *Univ. Bordeaux, CNRS, Bordeaux INP, IMB, UMR 5251, F-33400 Talence*
[c] *INRIA, F-33400 Talence*

Abstract

In this paper, numerical methods are developed and detailed in order to be able to compute the ablation of metallic thermal protection system. In this complex multi-physics problem, the thermal state inside a solid domain and a two-phase viscous flow have to be computed. Since the two fluid phases are non-miscible, an extension of the five-equation model to dissipative effects is considered. An operator splitting strategy is used to separate the different phenomena according to their own propagation speed. An implicit time integration is performed for the acoustic+dissipative step while the transport step is computed with an explicit scheme. The hyperbolic part of the acoustic+dissipative step is solved in a non-conservative form using a Godunov-type scheme based on a simple Riemann solver. A classical discretization is used for the dissipative terms, and also for the heat equation inside the solid domain. Several approaches are detailed in order to prevent the numerical diffusion of the material interface in the transport step. Finally, since moving grids are used to capture accurately the melting front, an ALE formulation of the numerical schemes for both fluid and solid domains is given in a multidimensional framework. A fluid-solid coupling algorithm is then proposed to compute such a complex multi-physics problem.
Numerical simulations show the validity and the robustness of the implicit-explicit scheme used for the discretization of the five-equation system. The last test case, namely the melting of an aluminium solid block by a lid-driven cavity filled with air, shows that the numerical tools developed here are robust enough to compute complex configurations involving a two-phase flow with high density ratios and a solid part.

Keywords: Two-phase flows, Compressible Navier-Stokes, Godunov-type schemes, ALE formulation, Fluid-Solid coupling, Ablation

1. Introduction

The present work takes place in the context of the atmospheric re-entry problem. This study can concern re-entry vehicles globally or partially made of metallic components, space debris for instance. During the re-entry phase, a solid undergoes a heating due to the friction of atmospheric gases. Conversion of kinetic energy to thermal energy leads to a sudden increase of the temperature of the object. This rise drives to a physical-chemical degradation of the thermal protection system, and to a boundary recession. Sublimation (injection of gas into the atmosphere) and fusion of the metallic part (creation of a liquid phase between the gas and the wall) are the main causes of the solid ablation during the re-entry phase. In order to simulate this very complex problem, a zonal approach is considered, see Fig 1. In the gas flow region, far from the object or near a wall made of carbon where the ablation process is driven by the sublimation, classical schemes can be used. Numerical simulations of the sublimation process have already been studied in [MB14, MC13, BNM10, Mul10, Lat13]. In the region near a metallic wall, the velocity of the gas is small and with the appearance of the liquid phase, the dynamics of the flow is very different. The presence of the liquid layer between the solid wall and the gas flow is usually not taken into account

*Corresponding author
**Retired fellow
Email address: simon.peluchon@cea.fr (S. Peluchon)

in the literature. The development of new numerical tools for the simulation of the liquid ablation seems to be in progress in [HSD$^+$19], but the molten phase is once again not considered.

The ablation of a metallic object during its reentry phase is a very complex phenomenon. A multi-physic computation is needed in order to handle such configurations. The thermal state inside the solid has to be determined while an accurate computation of the two-phase flow in the fluid region is mandatory since the melting process is driven by the heat flux at the wall. The computation of the two-phase flow resulting from the melting of the solid part is very challenging since the density ratio between the high enthalpy gas and the almost incompressible liquid is very important. Moreover, a fine mesh close to walls needs to be used in order to capture accurately viscous and thermal boundary layers. Implicit time integration are also required in order to overcome stability conditions related to those meshes. From our own experience, usual numerical schemes are not very robust to compute such two-phase flows when large time steps are considered. In the present paper, robust numerical schemes are described in order to simulate the melting process of a metallic material and the resulting two-phase flow. The numerical method described in this paper for the two-phase flow region is an extension of the scheme given in [PGM17] in which viscous effects were not taken into account in the fluid domain.

The modeling and computation of multiphase flows have been widely studied for the past decades. There are two main approaches to compute compressible flows with interfaces: sharp interface methods, and diffuse interface methods. In the first approach, the interface between the two media, considered as a sharp discontinuity, is followed explicitly and each phase can be computed with different models. In Lagrangian or Arbitrary Lagrangian-Eulerian methods, the mesh moves during the computation like the interface. Large distortions and interface topological changes can hardly be taken into account. Front capturing methods are Eulerian methods where the interface is reconstructed. In Level Set methods [OS88] the interface is located as the zero of an implicit function. In the Volume Of Fluid method [HN81], the interface is reconstructed from the volume fraction of each fluid. In the second approach, diffuse interface methods [BN86, MSNA02, ACK02, FBC$^+$11, KL10, SA99], based on an Eulerian mesh, allow numerical diffusion of the interface. The same equations are solved in the entire domain. In addition, these models allow the creation of new interfaces and topological changes during the simulation. Consequently, the diffusive interface approach is used in this work to handle the large deformation induced by the fusion of the metallic part. Those methods have already been studied by many authors. The seminal work of Baer and Nunziato [BN86] (see also [SW84]) introduces a pressure and velocity non-equilibrium model for two-phase flows. The model of Kapila et al. [KMB$^+$01] can be seen as the limit of instantaneous velocity and pressure relaxation, see [MG05, FL11]. In this case, a non-conservative term proportional to the divergence of the velocity appears in the equation of the volume fraction. This term describes the expansion/compression effects in case of a mixture. Several numerical schemes have been recently proposed for the Kapila et al. model or its variants [MG05, SPB09, LMNS13, PS14, LMSN14]. However, as suggested by some experiments, we assume that the liquid phase in our application will not disperse nor mix with the gas flow. Consequently, non-miscible fluids can be considered in this study and the non-conservative term of Kapila et al. model can be neglected. Indeed, at the continuous level, if the initial condition is made of two separated phases, then both Kapila et al. model and the five-equation model of [MSNA02, ACK02] give the same solution. It is only at the discrete level that differences can appear inside the small mixture zone due to the numerical diffusion. Therefore, a model based on the five-equation model [MSNA02, ACK02] is used in this work to capture the pure interface between the two fluids. A careful treatment of the numerical diffusion of the material interface is done in order to prevent the growth of the mixture zone between the gas and the liquid.

Viscous and thermal boundary layers need to be accurately computed in order to correctly give the heat flux at the wall. If the two phases are governed by Navier-Stokes equations, following Baer and Nunziato work, a seven-equation system can be constructed. A velocity and pressure relaxation procedure can be done [BN09] in order to derive a five-equation model with dissipative effects. This system is considered in the fluid domain.

A two-phase flow involving an almost incompressible liquid and a compressible gas is considered here. With the diffuse interface method, the same equations are solved in the entire domain, hence the liquid is modeled by a viscous compressible fluid in which the Mach number is very low. Several time scales are involved in this configuration: the scale of the fast acoustic waves, the scale of diffusive effects which both lead to an important CFL restriction on the time step for explicit schemes, and the scale of slow material waves. Usually, implicit numerical schemes allow to use large time scales and fine meshes to compute boundary layers. However, up to our knowledge, implicit schemes for two-phase flows simulations are not very robust with large CFL conditions. One of the main objectives of this work is to derive a robust scheme to compute two-phase flow with dissipative effects using large time steps.

Another difficulty is the lack of accuracy of the numerical schemes in the low Mach regime. This topic has been widely investigated in the literature, see [GV99, GM04, MG08, DJOR16, BDJP19] and the references therein. Preconditioned methods or specific corrections of the numerical flux have been developed in order to capture the low Mach limit [Tur87, TMD$^+$08, Rie11, Del10]. For single-phase flows in the low Mach regime, several implicit-explicit schemes have been proposed, like [DJY07, HJL12, CDK12], to resolve the material wave scale only. Another approach [CGK16, CGK17] is to use a splitting of the Euler equations between acoustic and transport systems. The acoustic system is resolved by an implicit scheme while the transport system is resolved by an explicit scheme. A low Mach fix based on a correction of the pressure flux is developed for the acoustic step. This approach is also used here.

Finally, since the melting front is moving during the ablation process, the numerical schemes developed for both fluid and solid domains have to deal with moving meshes and boundaries. The governing equations are therefore integrated over a moving control domain and an Arbitrary Lagrangian-Eulerian formulation of the numerical schemes is used. To ensure that uniform state flows are preserved by the numerical procedures while the mesh is deforming, the Geometrical Conservation Law must be satisfied at the discrete level.

In this paper, several numerical tools are proposed to handle those challenges: compute the thermal state inside the (moving) solid domain, simulate a viscous two-phase flow which involves large ratios of density, pressure and temperature, derive an implicit scheme in order to use large time steps, compute accurately boundary layers and second-order quantities like heat flux at the boundary of the domain, deal with an almost incompressible liquid as a compressible fluid by using a low Mach correction and prevent numerical diffusion of the liquid-gas interface. To overcome these challenges, the following numerical tools are needed. A classical implicit diffusion scheme is used for the heat equation inside the solid domain. For the fluid domain, an extension of the splitting strategy presented in [PGM17, CGK16, CGK17] to the five-equation system with dissipative effects is proposed. The splitting strategy is done with a Lagrange-Projection type [GR91] algorithm. The hyperbolic part of the acoustic+dissipative step is solved in a non-conservative form using a Godunov-type scheme based on a simple Riemann solver [Gal03]. The Riemann solver slopes are computed using exact positivity conditions for the solution. The same discretization as the solid is used for the dissipative terms. An implicit treatment of the acoustic+dissipative step allows large time steps that are based on the material waves velocity. An extension of the time-implicit scheme of [PGM17] is derived. Numerical fluxes of the hyperbolic part are first computed thanks to an autonomous and linear pressure-velocity sub-system. The specific volume can be directly updated while an iterative process is needed to compute the new internal energy. The transport step is then solved explicitly. Several approaches can be used in order to prevent numerical diffusion of the material interface between the gas flow and the liquid layer. Indeed, the usual upwind scheme for the transport step generates a large amount of numerical diffusion, and extends the mixture zone between the two phases. The anti-diffusive scheme of Kokh and Lagoutière [KL10] and the pseudo-random choice of Glimm [BHJ$^+$13, Col82] are used to prevent this diffusion. The global scheme for the fluid domain is conservative. Thus, the right shock speeds are obtained. An ALE formulation of the numerical schemes for both fluid and solid domains is given to handle the mesh deformation during the melting process. A fluid-solid coupling algorithm is also proposed to compute the complex multi-physics problem of liquid

ablation.

The outline of this paper is as follow. In the next section, governing equations for both solid and fluid domains are given. Jump relations at the interface between the fluid and the solid are also detailed. In section 3, the numerical schemes used to compute the thermal state inside and the two-phase flow in the fluid domain are presented. The Arbitrary Lagrangian Eulerian approach needed to compute the governing equations on a moving mesh is also detailed for both solid and fluid domains. A fluid-solid coupling algorithm is then presented in section 4. Finally, the extension of the splitting resolution to dissipative effects is verified in section 5. A final test case involving three phases is studied, namely the melting of an aluminium solid block by a lid-driven cavity filled with air.

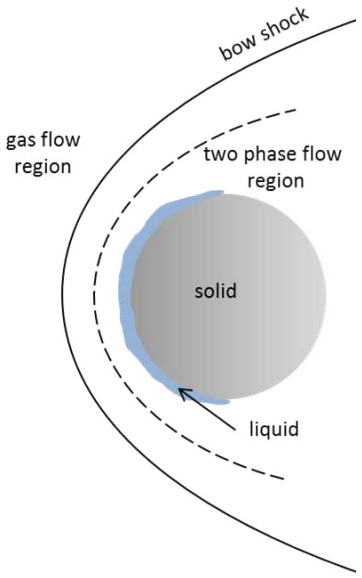

Figure 1: Description of the different phenomena occurring during the re-entry of a metallic debris.

2. Governing equations

2.1. Solid domain: heat equation

The unsteady thermal state of the solid domain is described by the heat equation

$$\partial_t \left(\rho_s \varepsilon_s\right) + \nabla \cdot \boldsymbol{q}_s = 0, \tag{1}$$

where ρ_s is the solid density and $\boldsymbol{q}_s$ the heat flux. The general form of the specific internal energy ε_s is given by $\varepsilon_s(T_s) = \int_{T_0}^{T_s} c_p(T')\,\mathrm{d}T'$, where T_s is the temperature inside the solid, T_0 a temperature of reference and c_p is the heat capacity. Here, c_p is assumed to be constant, therefore $\varepsilon_s = c_p(T_s - T_0)$. The thermal diffusion of the solid is supposed to be isotropic and the heat flux is given by the Fourier's law

$$\boldsymbol{q}_s = -\kappa_s \boldsymbol{\nabla} T_s,$$

where κ_s is the thermal conductivity of the solid. In addition, pyrolysis effects are not considered here, so the density of the solid is constant.

2.2. Fluid domain: five-equation system with dissipative effects

In our application, there is initially no liquid phase corresponding to molten solid in the fluid region and we assume that the gas flow will not mix with the liquid. Consequently, non-miscible fluids can be considered and the five-equation system of [MSNA02, ACK02] can be used in the fluid domain. Indeed, the non-conservative term of Kapila et al. model [KMB$^+$01] can be neglected, since at the continuous level, if the two fluid phases are not mixed at the initial time, both Kapila et al.

and the five-equation models give the same solution. An extension of the five-equation model is used in order to take into account the dissipative effects related to the viscosity and thermal conductivity of the fluid: this model is explained below.

The density, the internal energy, the pressure and the temperature of the two fluid phases $k = 1, 2$ are denoted by ρ_k, ε_k, p_k and T_k. Each fluid is equipped with an Equation Of State (EOS) given by $p_k = p_k(\rho_k, \varepsilon_k)$ and $\varepsilon_k = \varepsilon_k(\rho_k, T_k)$. The sound speed c_k of each phase is defined by $c_k^2 = \frac{\partial p_k}{\partial \rho_k}\Big|_{s_k}$, where s_k is the entropy.

Volume fraction z_k of each fluid is introduced such that the saturation relation $z_1 + z_2 = 1$ yields. In the sequel, the volume fraction of the first fluid is denoted by $z = z_1$. One can also introduce the mass fraction of the first fluid $y = \frac{\rho_1 z}{\rho}$. The mixture density ρ and mixture internal energy ε can be defined through the volume and mass fractions, the density and internal energy of each fluid

$$\begin{aligned} \rho &= z\rho_1 + (1-z)\rho_2, \\ \varepsilon &= y\varepsilon_1 + (1-y)\varepsilon_2. \end{aligned}$$

Both phases share the same velocity $\boldsymbol{u}$, and the same pressure p. The five-equation system with dissipative effect is given by [BN09]

$$\begin{cases} \partial_t \rho + \nabla \cdot (\rho \boldsymbol{u}) = 0, \\ \partial_t (\rho y) + \nabla \cdot (\rho y \boldsymbol{u}) = 0, \\ \partial_t (\rho \boldsymbol{u}) + \nabla \cdot (\rho \boldsymbol{u} \otimes \boldsymbol{u}) + \boldsymbol{\nabla} p = \nabla \cdot \mathsf{T}, \\ \partial_t (\rho E) + \nabla \cdot (\rho E \boldsymbol{u} + p\boldsymbol{u}) = \nabla \cdot (\mathsf{T}\boldsymbol{u}) - \nabla \cdot \boldsymbol{q}, \\ \partial_t z + \boldsymbol{u} \cdot \boldsymbol{\nabla} z = 0, \end{cases} \tag{2}$$

where $E = \varepsilon + \frac{|\boldsymbol{u}|^2}{2}$ is the total mixture energy, T the Cauchy stress tensor and $\boldsymbol{q}$ the heat flux.

The EOS associated to each phase is assumed to be given by the stiffened gas EOS, namely

$$\begin{aligned} p_k(\rho_k, \varepsilon_k) &= (\gamma_k - 1)\rho_k(\varepsilon_k - q_k) - \gamma_k \pi_k, \\ \varepsilon_k(\rho_k, T_k) &= q_k + c_{v,k} T_k + \frac{\pi_k}{\rho_k}, \end{aligned}$$

where $\gamma_k > 1$ is the adiabatic exponent, $\pi_k \geq 0$ a reference pressure and q_k an internal energy of reference. Heat capacity at constant volume is denoted by $c_{v,k}$. Using the isobaric closure relation [ACK02], namely $p_1(\rho_1, \epsilon_1) = p_2(\rho_2, \epsilon_2)$, and the definition of mixture internal energy ε, the pressure can be obtained as $p = (\gamma - 1)\,\rho(\varepsilon - q) - \gamma\pi$ where the mixture parameters γ, π and q are defined by

$$\begin{aligned} \frac{1}{\gamma(z) - 1} &= z\frac{1}{\gamma_1 - 1} + (1-z)\frac{1}{\gamma_2 - 1}, \\ \frac{\gamma(z)\pi(z)}{\gamma(z) - 1} &= z\frac{\gamma_1 \pi_1}{\gamma_1 - 1} + (1-z)\frac{\gamma_2 \pi_2}{\gamma_2 - 1}, \\ q(y) &= yq_1 + (1-y)q_2. \end{aligned} \tag{3}$$

In the general case, the mixture sound speed is given by [ACK02]

$$c^2 = \frac{1}{\xi} \sum_{k=1}^{2} y_k \xi_k c_k^2,$$

where ξ_k is the partial derivative $\frac{\partial(\rho_k \epsilon_k)}{\partial p}$, $\xi = \sum_{k=1}^{2} z_k \xi_k$ and c_k the sound speed of the pure fluid k. Since the speed of sound for a stiffened gas is given by $c_k^2 = \gamma_k \frac{p + \pi_k}{\rho_k}$, the mixture sound speed for the mixture of two stiffened gases reads

$$c^2 = \gamma \frac{p + \pi}{\rho}.$$

Viscous effects are taken into account by the symmetric Cauchy stress tensor T in the momentum and energy equations. Assuming that both phases are Newtonian fluids, viscous stress tensor is given by

$$\mathsf{T} = -\frac{2}{3}\mu\nabla\cdot\boldsymbol{u}\mathsf{I_d} + 2\mu\mathsf{D},$$

where the mixture viscosity $\mu = \sum_{k=1}^{2} z_k\mu_k$ and $\mathsf{D} = \frac{1}{2}(\nabla\boldsymbol{u} + \nabla^T\boldsymbol{u})$ is strain rate tensor.

The heat flux $\boldsymbol{q} = \sum_{k=1}^{2} z_k\boldsymbol{q}_k$ in the total energy equation takes in account the effect of thermal dissipation. As for the solid domain, the thermal diffusion of phase k is supposed to be isotropic and the heat flux is given by the Fourier's law $\boldsymbol{q}_k = -\kappa_k\boldsymbol{\nabla}T_k$ where κ_k is the thermal conductivity of phase k. However, in the case of two-phase flows where the fluids are separated, the terms $\boldsymbol{\nabla}T_k$ are not clearly defined around the material interface. Therefore, the mixture heat flux is assumed here to be given by a Fourier's law $\boldsymbol{q} = -\kappa\boldsymbol{\nabla}T$ with a mixture thermal conductivity $\kappa = z\kappa_1 + (1-z)\kappa_2$ and where T is a mixture temperature. Note that for continuous solutions where the two phases are initially separated, the two definitions of the mixture heat flux give the same solutions. As for the Kapila's term [KMB+01] in the evolution equation of the volume fraction, differences can appear inside the small mixture zone due to the numerical diffusion at the discrete level.

In this paper, initial conditions made of two separated phases are considered, thus if there is no numerical diffusion of the interface, e.g. with the Glimm's random choice method in the transport step, see section 3.4.2, the choice of the definition of the heat flux will have no impact. If a mixture zone appears due to the numerical diffusion, differences in terms the global solution are expected to remain small.

To define the mixture temperature T which appears in the definition of the heat flux $\boldsymbol{q} = -\kappa\boldsymbol{\nabla}T$, the relation of mixture internal energy is used

$$\varepsilon = y\varepsilon_1 + (1-y)\varepsilon_2. \tag{4}$$

With the stiffened gas EOS considered here, the internal energy of a phase k is given by

$$\varepsilon_k(T_k,\rho_k) = q_k + c_{v_k}T_k + \frac{\pi_k}{\rho_k}.$$

Introducing the mixture heat capacity $c_v = \sum_k y_k c_{v_k}$, and the mixture temperature

$$T = \frac{1}{c_v}\sum_{k=1}^{2} y_k c_{v_k} T_k, \tag{5}$$

the mixture internal energy (4) reads

$$\varepsilon(T,\rho_1,\rho_2,z,y) = q(y) + c_v T + \sum_{k=1}^{2} y_k\frac{\pi_k}{\rho_k}, \tag{6}$$

where $q(y) = yq_1 + (1-y)q_2$ is the mixture parameter defined by the isobaric closure (3).

Finally, in the study, viscosity coefficient μ_k, thermal conductivity κ_k and heat capacity c_v of each phase are taken constant. It is probably not difficult to overcome this assumption even if it is not done here.

Remark 1
Another definition of the mixture temperature based on the mixture entropy of the five-equation system can be used. However, numerical results presented in section 5.1 show that this choice generates numerical artifacts on the discrete solution inside the mixture zone.

2.3. Boundary conditions at the fluid-solid interface

To determine the coupling conditions, mass and energy balances are written as jump conditions at the interface between the fluid and the solid domains. The solid domain is seen as a compressible fluid with zero velocity and stress tensor. Therefore, two compressible fluids separated by a moving interface are considered.

From those governing equations, jump relations at the wall can be defined for the mass and energy conservation equations.

Mass balance

Let us recall that the density of the solid domain ρ_s is assumed to be constant and its velocity equal to zero. We denote by $\boldsymbol{n}$ the normal to the interface (directed to the fluid) and $w_{itf} = \boldsymbol{w}_{itf} \cdot \boldsymbol{n}$ the normal (recession) velocity at the wall. Then the Rankine-Hugoniot condition gives

$$\rho_f(\boldsymbol{u}_f - \boldsymbol{w}_{itf}) \cdot \boldsymbol{n} = -\rho_s \boldsymbol{w}_{itf} \cdot \boldsymbol{n}, \tag{7}$$

where ρ_f and $\boldsymbol{u}_f$ are the fluid density and velocity. We denote by $\dot{m} = \rho_f(\boldsymbol{u}_f - \boldsymbol{w}_{itf}) \cdot \boldsymbol{n}$ the mass flux through the solid wall, and we can deduce

$$\boldsymbol{w}_{itf} \cdot \boldsymbol{n} = -\frac{\dot{m}}{\rho_s}, \tag{8}$$

$$\boldsymbol{u}_f \cdot \boldsymbol{n} = \left(1 - \frac{\rho_s}{\rho_f}\right) \boldsymbol{w}_{itf} \cdot \boldsymbol{n}. \tag{9}$$

When we know the mass flux $\dot{m}$, this mass balance allows us to determine the normal recession velocity at the wall w_{itf} as well as the injection velocity of the liquid phase inside the fluid $\boldsymbol{u}_f \cdot \boldsymbol{n}$. In this work, we assume that there is no slip at the wall and the injection of the liquid phase inside the fluid occurs according the normal at the interface, *i.e.* $\boldsymbol{u}_f = u_f \boldsymbol{n}$.

In the last numerical test case of this paper, the melting of an aluminium solid block is studied. In this case, the density ratio between the solid part and the molten metal is equal to 1.08. Thus, the injection velocity u_f (9) and the interface velocity w_{itf} are of opposite signs. Note that in the particular case where $\rho_s = \rho_f$, the injection velocity is equal to zero. There is therefore adhesion of liquid on the mobile wall.

Energy balance

Stefan condition [Ste91] is used for the energy balance. The mass flux $\dot{m}$ is determined from the solid and fluid heat fluxes at the interface between the two domains. Energy balance reads

$$\dot{m}L = \kappa_f \frac{\partial T_f}{\partial \boldsymbol{n}} - \kappa_s \frac{\partial T_s}{\partial \boldsymbol{n}}. \tag{10}$$

where L is the latent heat of melting.

Governing equations for the fluid and solid domains and the boundary conditions at the wall have been described. In the next section, the numerical schemes for each domain are given.

3. Numerical scheme

Without loss of generality, a two-dimensional problem discretized over a structured mesh (curvilinear grid) is considered. In order to simplify the computation of mass and energy balances, conforming mesh for the fluid and solid domains are used. Let us denote by $\Omega_{l,m}$ a cell of our mesh, $\Gamma_{l+1/2,m}$ (resp. $\Gamma_{l,m+1/2}$) the face of the cell $\Omega_{l,m}$ toward the first direction of the mesh (resp. the second one) and $\boldsymbol{n}_{l+1/2,m}$ (resp. $\boldsymbol{n}_{l,m+1/2}$) the unit vector normal to $\Gamma_{l+1/2,m}$ (resp. $\Gamma_{l,m+1/2}$), see Fig. 2. The area of a cell $\Omega_{l,m}$ is denoted by $\left|\Omega_{l,m}\right|$. Likewise, the length of a face $\Gamma_{l+1/2,m}$ is denoted by $\left|\Gamma_{l+1/2,m}\right|$.

For the sake of clarity, a one-index notation $\boldsymbol{i} = (l, m)$ is used most of the time for two-dimensional meshes. The area of a cell $\Omega_{\boldsymbol{i}}$ is therefore denoted by $|\Omega_{\boldsymbol{i}}|$ while the quantities defined on the face between the cells $\Omega_{\boldsymbol{i}}$ and $\Omega_{\boldsymbol{j}}$ will be denoted by the subscript $\boldsymbol{ij}$.

Let $\Delta t > 0$ be the time step. Finite-volume methods are used, in which the approximate value of ϕ within the cell $\Omega_{\boldsymbol{i}}$ at time t^n is denoted by $\phi_{\boldsymbol{i}}^n$.

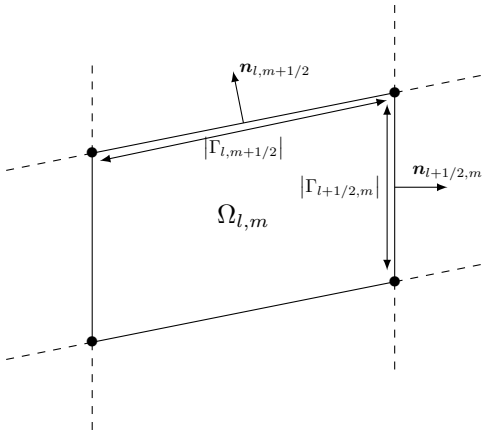

Figure 2: Two-index notations inside a cell for a 2D structured mesh.

3.1. Discretization of the dissipative terms

A classical direct implicit scheme is used to compute the heat equation inside the solid domain. The same discretization will be used for the dissipative terms of the two-phase flow system (2). For the sake of simplicity, the diffusion equation of a quantity θ

$$\partial_t \theta = \nabla \cdot (\lambda \boldsymbol{\nabla} \theta)\,, \tag{11}$$

is used here to describe the discretization of the dissipative terms. The parameter λ can be space-dependent. The extension for Navier-Stokes equations is straightforward.

The construction of the numerical scheme for the diffusion equation (11) is not detailed here. It is based on a transformation between the physical curvilinear structured grid and a Cartesian reference grid. The numerical scheme reads

$$\theta_{\boldsymbol{i}}^{n+1} = \theta_{\boldsymbol{i}}^{n} + \frac{\Delta t}{|\Omega_{\boldsymbol{i}}|} \sum_{\boldsymbol{j} \in v(\boldsymbol{i})} \left(\frac{\lambda}{|\Omega|} \right)_{\boldsymbol{ij}} \left((\boldsymbol{n}\,|\Gamma|)_{\boldsymbol{ij}} \, (\theta_{\boldsymbol{j}}^{n+1} - \theta_{\boldsymbol{i}}^{n+1}) + (\boldsymbol{t}\,|\Gamma|)_{\boldsymbol{ij}} (\theta_{\boldsymbol{ij}}^{A} - \theta_{\boldsymbol{ij}}^{B}) \right) \cdot (\boldsymbol{n}\,|\Gamma|)_{\boldsymbol{ij}}, \tag{12}$$

where the right-hand side is a sum of numerical fluxes across the edges between cell $\boldsymbol{i}$ and its neighbouring cells, whose numbers are denoted by $\boldsymbol{j}$ and are stored in $v(\boldsymbol{i})$. The different terms of the numerical flux are described later. Note that each flux can be split into two contributions: a normal contribution involving the temperatures $\theta_{\boldsymbol{i}}$ and $\theta_{\boldsymbol{j}}$ of cells on both sides of the interface and a transverse contribution where the values of the auxiliary nodes A and B appear, see figure 3.

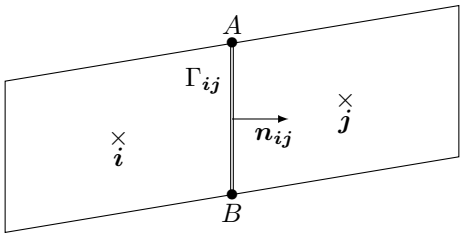

Figure 3: Notations used in the definition of the numerical flux for the dissipation equation for the edge $\Gamma_{\boldsymbol{ij}}$ between cells $\boldsymbol{i}$ and $\boldsymbol{j}$.

A harmonic mean between the values on both sides of the edge is used to define the term $\left(\frac{\lambda}{|\Omega|}\right)_{\boldsymbol{ij}}$, namely

$$\left(\frac{\lambda}{|\Omega|} \right)_{\boldsymbol{ij}} = 2 \frac{\lambda_{\boldsymbol{i}} \lambda_{\boldsymbol{j}}}{\lambda_{\boldsymbol{i}} \left|\Omega_{\boldsymbol{j}}\right| + \lambda_{\boldsymbol{j}} \left|\Omega_{\boldsymbol{i}}\right|}.$$

In contrast to the arithmetic mean, using a harmonic mean preserves the piecewise linear fields [Cha04].

For the normal contribution, the term $(\boldsymbol{n}\,|\Gamma|)_{\boldsymbol{ij}}$ is equal to unitary normal of the edge $\boldsymbol{n}_{\boldsymbol{ij}}$ times the length of the edge $|\Gamma_{\boldsymbol{ij}}|$. The term $(\boldsymbol{t}\,|\Gamma|)_{\boldsymbol{ij}}$ corresponds to the transverse contribution. To define this term, a two-index notation is used, see Fig. 4. Thus, if the cells $\boldsymbol{i}$ and $\boldsymbol{j}$ are respectively denoted by (l, m) and $(l+1, m)$, one has

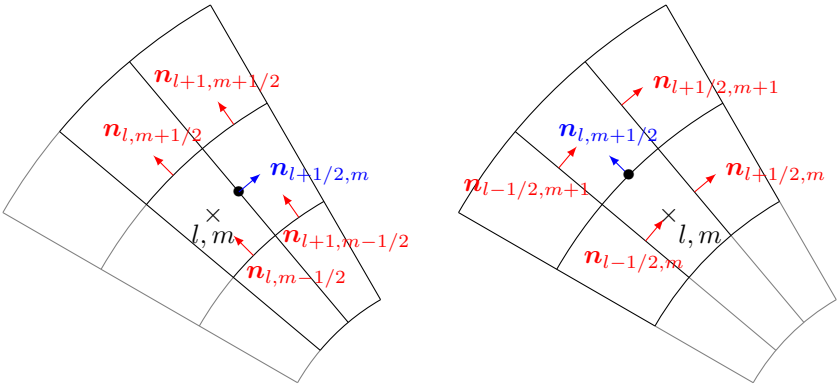

(a) edge $l + 1/2, m$ (b) edge $l, m + 1/2$

Figure 4: Contributions in order to compute metric coefficients on a given edge.

$$(\boldsymbol{t}\,|\Gamma|)_{\boldsymbol{ij}} = (\boldsymbol{t}\,|\Gamma|)_{l+1/2,m} = \frac{1}{4}\left((\boldsymbol{n}\,|\Gamma|)_{l,m+1/2} + (\boldsymbol{n}\,|\Gamma|)_{l+1,m+1/2} + (\boldsymbol{n}\,|\Gamma|)_{l,m-1/2} + (\boldsymbol{n}\,|\Gamma|)_{l+1,m-1/2}\right).$$

Note that the vector $\boldsymbol{t}$ is not necessarily orthogonal to the normal $\boldsymbol{n}$.

Finally, the values of the auxiliary nodes A and B are needed to describe completely the numerical flux (12). For the numerical scheme used here, the values of the auxiliaries points are defined as the average of the four temperatures around the node. Namely, for the edge $\Gamma_{l+1/2,m}$, the nodal values are given by

$$\theta^A_{l+1/2,m} = \frac{1}{4}\left(\theta^{n+1}_{l,m} + \theta^{n+1}_{l+1,m} + \theta^{n+1}_{l,m+1} + \theta^{n+1}_{l+1,m+1}\right),$$
$$\theta^B_{l+1/2,m} = \frac{1}{4}\left(\theta^{n+1}_{l,m-1} + \theta^{n+1}_{l+1,m-1} + \theta^{n+1}_{l,m} + \theta^{n+1}_{l+1,m}\right).$$

For a non Cartesian structured mesh, this numerical scheme (12) gives a nine-point stencil. However, in the case of a Cartesian mesh, the numerical scheme reduces to a five-point scheme, see figure 5. Indeed, the term $(\boldsymbol{n}\,|\Gamma|)_{\boldsymbol{ij}} \cdot (\boldsymbol{t}\,|\Gamma|)_{\boldsymbol{ij}}$ inside the numerical flux (12) is equal to zero for a Cartesian grid. If the Cartesian mesh is also regular, *i.e.* $|\Omega_{\boldsymbol{i}}| = |\Omega| = (\Delta x)^2$ for all cells, the scheme give the classical five-point diffusion scheme

$$\theta^{n+1}_{\boldsymbol{i}} = \theta^n_{\boldsymbol{i}} + \frac{\Delta t}{(\Delta x)^2} \sum_{\boldsymbol{j}\in v(\boldsymbol{i})} \lambda_{\boldsymbol{ij}} \left(\theta^{n+1}_{\boldsymbol{j}} - \theta^{n+1}_{\boldsymbol{i}}\right).$$

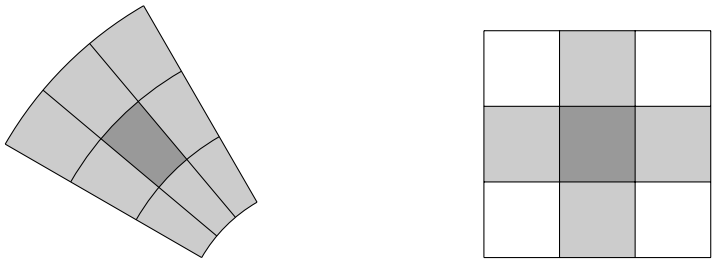

Figure 5: Discretization of the dissipative terms. Nine-point stencil for a curvilinear grid (left) and five-point stencil for a Cartesian mesh (right).

Remark 2
With this scheme, second-order accuracy will be reached with this discretization of the diffusion terms for curvilinear grids without large deformation. However, the maximum principle is not verified. Recent works [LP09, BL15, Wu17, ZSW17] on diffusion schemes using nonlinear methods ensure the positivity of the solution.

3.2. An operator splitting strategy for the fluid domain

For the fluid domain, the idea is to separate the different phenomena according to their own propagation speed as in [GR91, CGK16, KL10, CNPT10]. An acoustic-dissipative-transport operator splitting strategy is therefore used to approximate the solution of the five-equation system with dissipative effects (2).

Fine meshes along the walls need to be used in order to be able to compute dissipative terms accurately. The characteristic times of thermal and viscous diffusion are proportional to the square of the characteristic length of the mesh, which implies very large constraints if an explicit scheme is used. In the acoustic-transport splitting strategy [PGM17, CGK16], an implicit scheme is used for the acoustic step while the transport step is solved explicitly. This is why we choose to put the dissipative terms with the acoustic part of the splitting.

The first system takes into account the propagation of the acoustic waves and the effects of the dissipative terms. This system called the acoustic+dissipative system reads

$$\begin{cases} \partial_t \rho & + \rho \nabla \cdot \boldsymbol{u} & = 0, \\ \partial_t (\rho y) & + \rho y \nabla \cdot \boldsymbol{u} & = 0, \\ \partial_t (\rho \boldsymbol{u}) & + \rho \boldsymbol{u} \nabla \cdot \boldsymbol{u} + \boldsymbol{\nabla} p & = \nabla \cdot \mathsf{T}, \\ \partial_t (\rho E) & + \rho E \nabla \cdot \boldsymbol{u} + \nabla \cdot (p \boldsymbol{u}) & = \nabla \cdot (\mathsf{T} \boldsymbol{u}) - \nabla \cdot \boldsymbol{q}, \\ \partial_t z & & = 0. \end{cases} \tag{13}$$

An implicit scheme is proposed for this step in order to overcome CFL restrictions.

The second system is called the transport system and it takes into account the propagation of material waves through the fluid. It is given by

$$\begin{cases} \partial_t \rho & + \boldsymbol{u} \cdot \boldsymbol{\nabla} \rho & = 0, \\ \partial_t (\rho y) & + \boldsymbol{u} \cdot \boldsymbol{\nabla} (\rho y) & = 0, \\ \partial_t (\rho \boldsymbol{u}) & + \boldsymbol{u} \cdot \boldsymbol{\nabla} (\rho u) & = 0, \\ \partial_t (\rho E) & + \boldsymbol{u} \cdot \boldsymbol{\nabla} (\rho E) & = 0, \\ \partial_t z & + \boldsymbol{u} \cdot \boldsymbol{\nabla} z & = 0. \end{cases} \tag{14}$$

The overall splitting algorithm for a time step between t^n and t^{n+1} reads

1. **Acoustic+dissipative step:** From a state $(\rho, \rho y, \rho \boldsymbol{u}, \rho E, z)^n$, compute the approximation of the acoustic system with dissipative effects (13) denoted by $(\rho, \rho y, \rho u, \rho e, z)^\dagger$.

2. **Transport step:** Find the fluid state $(\rho, \rho y, \rho u, \rho e, z)^{n+1}$ by solving the transport system (14) with the initial state $(\rho, \rho y, \rho u, \rho e, z)^\dagger$.

This kind of algorithm has been already used in the literature with an implicit treatment of the first step for gas dynamic [CGK16], two-phase flow models such as Homogeneous Relaxation Model and Homogeneous Equilibrium Model [CGK17], or the five-equation system (without dissipative effects) [PGM17]. Fully explicit schemes have also been developed for the inviscid five-equation model by [FBC$^+$11, KL10] and for the Kapila et al. two-phase flow model by [EDKT17].

Numerical schemes for each step are described in the next section. Note that the transport step is not modified by taking dissipative effects into account as compared to [PGM17].

3.3. Acoustic+dissipative step

3.3.1. Explicit formulation of the acoustic step with the dissipation terms

First, the non-conservative system (13) is written differently. The second, third and fourth equations are combined with the evolution equation of the mixture density. Then, the first equation is divided by the square of the mixture density.

Finally, the acoustic+dissipative system reads

$$\begin{cases} \partial_t \vartheta - \vartheta \nabla \cdot \boldsymbol{u} & = 0, \\ \partial_t y & = 0, \\ \partial_t \boldsymbol{u} + \vartheta \boldsymbol{\nabla} p & = \vartheta \nabla \cdot \mathsf{T}, \\ \partial_t E + \vartheta \nabla \cdot (p\boldsymbol{u}) & = \vartheta \nabla \cdot (\mathsf{T}\boldsymbol{u}) - \vartheta \nabla \cdot \boldsymbol{q}, \\ \partial_t (\vartheta z) - z\vartheta \nabla \cdot \boldsymbol{u} = 0, \end{cases} \tag{15}$$

where $\vartheta = \frac{1}{\rho}$ is the specific volume.

Although this system is written in a non-conservative form, a suitable numerical approximation can be derived. Moreover, the global scheme for the five-equation system (13) will be conservative. A Godunov-type scheme based on an approximate Riemann solver is used for the hyperbolic part [PGM17, Gal03]. It is a simple Riemann solver [Gal00, Gal03, Bou04] using two intermediate states. Exact positivity conditions for the density, the internal energy and the sound speed are used to compute the Riemann solver slopes, denoted by $\bar{C}^-$ and $\bar{C}^+$.

The explicit numerical scheme formally reads

$$\begin{aligned} \vartheta_{\boldsymbol{i}}^{\dagger} &= \vartheta_{\boldsymbol{i}}^{n} + \frac{\Delta t}{|\Omega_{\boldsymbol{i}}|} \vartheta_{\boldsymbol{i}}^{n} \sum_{\boldsymbol{j} \in v(\boldsymbol{i})} |\Gamma_{\boldsymbol{ij}}| \, \bar{u}_{\boldsymbol{ij}}^{n}, \\ y_{\boldsymbol{i}}^{\dagger} &= y_{\boldsymbol{i}}^{n}, \\ \boldsymbol{u}_{\boldsymbol{i}}^{\dagger} &= \boldsymbol{u}_{\boldsymbol{i}}^{n} - \frac{\Delta t}{|\Omega_{\boldsymbol{i}}|} \vartheta_{\boldsymbol{i}}^{n} \left(\sum_{\boldsymbol{j} \in v(\boldsymbol{i})} |\Gamma_{\boldsymbol{ij}}| \, \bar{p}_{\boldsymbol{ij}}^{n} - \nabla_{\boldsymbol{i}} \cdot \mathsf{T}^{n} \right), \\ E_{\boldsymbol{i}}^{\dagger} &= E_{\boldsymbol{i}}^{n} - \frac{\Delta t}{|\Omega_{\boldsymbol{i}}|} \vartheta_{\boldsymbol{i}}^{n} \left(\sum_{\boldsymbol{j} \in v(\boldsymbol{i})} |\Gamma_{\boldsymbol{ij}}| \, \bar{p}_{\boldsymbol{ij}}^{n} \bar{u}_{\boldsymbol{ij}}^{n} - \nabla_{\boldsymbol{i}} \cdot (\mathsf{T}^{n} \boldsymbol{u}^{n}) + \nabla_{\boldsymbol{i}} \cdot \boldsymbol{q}^{n} \right), \\ z_{\boldsymbol{i}}^{\dagger} &= z_{\boldsymbol{i}}^{n}, \end{aligned}$$

where $\nabla_{\boldsymbol{i}} \cdot \bullet$ denotes the discretization of dissipative terms, see section 3.1. Note that the volume and mass fractions remain constant during this step. Let us recall that the normal velocity and the pressure on the edge $\Gamma_{\boldsymbol{ij}}$ are given by

$$\begin{aligned} \bar{u}_{\boldsymbol{ij}}^{n} &= \frac{\bar{C}_{\boldsymbol{ij}}^{-} \boldsymbol{u}_{\boldsymbol{i}}^{n} + \bar{C}_{\boldsymbol{ij}}^{+} \boldsymbol{u}_{\boldsymbol{j}}^{n}}{\bar{C}_{\boldsymbol{ij}}^{-} + \bar{C}_{\boldsymbol{ij}}^{+}} \cdot \boldsymbol{n}_{\boldsymbol{ij}} - \frac{p_{\boldsymbol{j}}^{n} - p_{\boldsymbol{i}}^{n}}{\bar{C}_{\boldsymbol{ij}}^{-} + \bar{C}_{\boldsymbol{ij}}^{+}}, \\ \bar{p}_{\boldsymbol{ij}}^{n} &= \frac{\bar{C}_{\boldsymbol{ij}}^{+} p_{\boldsymbol{i}}^{n} + \bar{C}_{\boldsymbol{ij}}^{-} p_{\boldsymbol{j}}^{n}}{\bar{C}_{\boldsymbol{ij}}^{-} + \bar{C}_{\boldsymbol{ij}}^{+}} - \frac{\bar{C}_{\boldsymbol{ij}}^{-} \bar{C}_{\boldsymbol{ij}}^{+}}{\bar{C}_{\boldsymbol{ij}}^{-} + \bar{C}_{\boldsymbol{ij}}^{+}} \left(\boldsymbol{u}_{\boldsymbol{j}}^{n} - \boldsymbol{u}_{\boldsymbol{i}}^{n} \right) \cdot \boldsymbol{n}_{\boldsymbol{ij}}, \end{aligned} \tag{16}$$

see [PGM17, Gal03].

Remark 3
Godunov-type schemes are not accurate in the low Mach regime. The low Mach correction of Chalons et al. [CGK16] is used in order to capture the incompressible limit inside the liquid layer. Only the non-centered term of the pressure flux is modified and reads

$$\bar{p}_{\boldsymbol{ij}}^{n} = \frac{\bar{C}_{\boldsymbol{ij}}^{+} p_{\boldsymbol{i}}^{n} + \bar{C}_{\boldsymbol{ij}}^{-} p_{\boldsymbol{j}}^{n}}{\bar{C}_{\boldsymbol{ij}}^{-} + \bar{C}_{\boldsymbol{ij}}^{+}} - \theta_{\boldsymbol{ij}} \frac{\bar{C}_{\boldsymbol{ij}}^{-} \bar{C}_{\boldsymbol{ij}}^{+}}{\bar{C}_{\boldsymbol{ij}}^{-} + \bar{C}_{\boldsymbol{ij}}^{+}} \left(\boldsymbol{u}_{\boldsymbol{j}}^{n} - \boldsymbol{u}_{\boldsymbol{i}}^{n} \right) \cdot \boldsymbol{n}_{\boldsymbol{ij}},$$

where $\theta_{\boldsymbol{ij}}$ is equal to the local Mach number if the flow is subsonic, namely $\theta_{\boldsymbol{ij}} = \min\left(\frac{|\bar{u}_{\boldsymbol{ij}}^{n}|}{\max(c_{\boldsymbol{i}}, c_{\boldsymbol{j}})}, 1 \right)$.

We also remind that the mixture heat flux $\boldsymbol{q}$ is supposed to be given by a Fourier's law $\boldsymbol{q} = -\kappa \boldsymbol{\nabla} T$ where $\kappa = z\kappa_1 + (1-z)\kappa_2$ and T is the mixture temperature

$$T = \frac{1}{c_v} \sum_{k=1}^{2} y_k c_{v_k} T_k. \tag{17}$$

The stability conditions for the explicit scheme of the acoustic+dissipative step depends on three contributions. In the one-dimensional case, they are given by

- acoustic condition

$$\frac{\Delta t}{\Delta x}\max_{i\in\mathbb{Z}}\left(\frac{\bar{C}^-_{i+\frac{1}{2}}+\bar{C}^+_{i-\frac{1}{2}}}{\rho_i^n}\right)\leq 1, \tag{18}$$

- viscous diffusion condition

$$\frac{\Delta t}{\Delta x^2}\max_{i\in\mathbb{Z}}\left(\frac{\mu_i}{\rho_i^n}\right)\leq \frac{1}{2}, \tag{19}$$

- thermal diffusion condition

$$\frac{\Delta t}{\Delta x^2}\max_{i\in\mathbb{Z}}\left(\frac{\kappa_i}{\rho_i^n c_{v_i}}\right)\leq \frac{1}{2}. \tag{20}$$

Those CFL conditions can be very restrictive in practice, especially when refined meshes close to walls are used to capture viscous and thermal boundary layers. Therefore, an implicit formulation of the acoustic+dissipative step is performed.

3.3.2. Implicit treatment for the acoustic+dissipative step

For the implicit treatment of the acoustic step with dissipation terms, an extension of the algorithm denoted by IM1 in [PGM17] for the hyperbolic part of the five-equation system is used. Since the numerical flux of the hyperbolic part depends only on pressure and velocity, the idea was to solve a simpler sub-system in order to find a prediction of those quantities. This velocity-pressure system appears to be linear and if the Riemann solver slopes $\bar{C}^-$ and $\bar{C}^+$ are equal, the IM1 method is equivalent to the scheme derived by Chalons et al. [CGK16, CGK17]. If the dissipation terms are taken into account, an additional assumption is made by neglecting some terms in the pressure evolution equation used for the resolution of the velocity-pressure system. This will allow us to have an linear and autonomous system. Once this linear system is solved, the specific volume of the mixture can be directly updated. On the contrary, because of the term related to the heat flux, the mixture energy cannot be directly updated. To find the new energy, the heat flux is once again supposed to be given by a Fourier's law with mixture thermal conductivity and mixture temperature based on the definition of the mixture internal energy. The energy equation is then solved using a Newton-Raphson method written in terms of mixture temperature.

All these steps are detailed below.

Resolution of the velocity-pressure system

In order to compute the numerical fluxes of the hyperbolic part of the acoustic step, a velocity-pressure sub-system needs to be solved. The evolution equation for the velocity reads

$$\partial_t \boldsymbol{u} + \vartheta \boldsymbol{\nabla} p = \vartheta \nabla\cdot \mathsf{T}, \tag{21}$$

while the evolution equation for the pressure is given by

$$\partial_t p + C^2\vartheta\nabla\cdot\boldsymbol{u} = \frac{\mathsf{T}:\mathsf{D}-\nabla\cdot\boldsymbol{q}}{\rho\sum_k y_k \left.\frac{\partial \varepsilon_k}{\partial p}\right|_{\rho_k}}, \tag{22}$$

where $C=\rho c$ is the Lagrangian sound speed. It can be shown that the second term of the right-hand side is related to the thermal expansion of the fluid is the low Mach regime. However, in the scope of our application, temperature variations of the (incompressible) liquid phase are small as compared to the gas one. It will be neglected here. Moreover, the first term of the right-hand side of (22) contains non linear terms that make the numerical solving difficult. Although it can be taken into account in a non-linear way, this term will be neglected too.

Finally, the following velocity-pressure system is used to predict the numerical fluxes of the hyperbolic part

$$\begin{cases} \partial_t \boldsymbol{u} + \vartheta \boldsymbol{\nabla} p \quad\quad = \vartheta \nabla \cdot \mathsf{T}, \\ \partial_t p \; + C^2 \vartheta \nabla \cdot \boldsymbol{u} = 0. \end{cases} \tag{23}$$

This simplification is important from a practical and numerical point of view since the velocity-pressure system is still linear and autonomous. The impact of those simplifications can be estimated by comparing the explicit and implicit treatment of the acoustic+dissipative step: the numerical validations given in section 5 show that those assumptions are acceptable.

An implicit formulation of this system (23) is then given by

$$\begin{aligned} \boldsymbol{u}_{\boldsymbol{i}}^{\dagger} &= \boldsymbol{u}_{\boldsymbol{i}}^{n} - \frac{\Delta t}{|\Omega_{\boldsymbol{i}}|} \vartheta_{\boldsymbol{i}}^{n} \left(\sum_{\boldsymbol{j} \in v(\boldsymbol{i})} |\Gamma_{\boldsymbol{ij}}| \, \bar{p}_{\boldsymbol{ij}}^{\dagger} - \nabla_{\boldsymbol{i}} \cdot \mathsf{T}^{\dagger} \right), \\ p_{\boldsymbol{i}}^{\dagger} &= p_{\boldsymbol{i}}^{n} - \frac{\Delta t}{|\Omega_{\boldsymbol{i}}|} \vartheta_{\boldsymbol{i}}^{n} (C_{\boldsymbol{i}}^{n})^2 \sum_{\boldsymbol{j} \in v(\boldsymbol{i})} |\Gamma_{\boldsymbol{ij}}| \, \bar{u}_{\boldsymbol{ij}}^{\dagger}, \end{aligned} \tag{24}$$

where

$$\begin{aligned} \bar{u}_{\boldsymbol{ij}}^{\dagger} &= \frac{\bar{C}_{\boldsymbol{ij}}^{-} \boldsymbol{u}_{\boldsymbol{i}}^{\dagger} + \bar{C}_{\boldsymbol{ij}}^{+} \boldsymbol{u}_{\boldsymbol{j}}^{\dagger}}{\bar{C}_{\boldsymbol{ij}}^{-} + \bar{C}_{\boldsymbol{ij}}^{+}} \cdot \boldsymbol{n}_{\boldsymbol{ij}} - \frac{p_{\boldsymbol{j}}^{\dagger} - p_{\boldsymbol{i}}^{\dagger}}{\bar{C}_{\boldsymbol{ij}}^{-} + \bar{C}_{\boldsymbol{ij}}^{+}}, \\ \bar{p}_{\boldsymbol{ij}}^{\dagger} &= \frac{\bar{C}_{\boldsymbol{ij}}^{+} p_{\boldsymbol{i}}^{\dagger} + \bar{C}_{\boldsymbol{ij}}^{-} p_{\boldsymbol{j}}^{\dagger}}{\bar{C}_{\boldsymbol{ij}}^{-} + \bar{C}_{\boldsymbol{ij}}^{+}} - \frac{\bar{C}_{\boldsymbol{ij}}^{-} \bar{C}_{\boldsymbol{ij}}^{+}}{\bar{C}_{\boldsymbol{ij}}^{-} + \bar{C}_{\boldsymbol{ij}}^{+}} \left(\boldsymbol{u}_{\boldsymbol{j}}^{\dagger} - \boldsymbol{u}_{\boldsymbol{i}}^{\dagger} \right) \cdot \boldsymbol{n}_{\boldsymbol{ij}}. \end{aligned} \tag{25}$$

Like in the inviscid case, values of the Riemann solver slopes and of Lagrangian sound speed $C_{\boldsymbol{i}}$ are frozen at time t^n. Then (24) is a linear system that can be written as

$$\left(\mathsf{I_d} + \frac{\Delta t}{|\Omega|} \mathsf{M} \right) \boldsymbol{W}^{\boldsymbol{u}p^{\dagger}} = \boldsymbol{W}^{\boldsymbol{u}p^{n}}, \tag{26}$$

where vector of velocity and pressure unknowns is denoted by $\boldsymbol{W}^{\boldsymbol{u}p} = (\boldsymbol{u}_{\boldsymbol{i}}, p_{\boldsymbol{i}})_{\boldsymbol{i}}^{T}$ and M is a nine-diagonal block matrix on a two-dimensional curvilinear mesh.

Specific volume update

Once the velocity-pressure sub-system is solved, numerical fluxes $\bar{u}_{\boldsymbol{ij}}^{\dagger}$ and $\bar{p}_{\boldsymbol{ij}}^{\dagger}$ can be derived from the equation (25). The evolution equation for specific volume is then given by

$$\vartheta_{\boldsymbol{i}}^{\dagger} = \vartheta_{\boldsymbol{i}}^{n} - \frac{\Delta t}{|\Omega_{\boldsymbol{i}}^{n}|} \vartheta_{\boldsymbol{i}}^{n} \sum_{\boldsymbol{j} \in v(\boldsymbol{i})} |\Gamma_{\boldsymbol{ij}}| \, \bar{\boldsymbol{u}}_{\boldsymbol{ij}}^{\dagger}.$$

The value of the new specific volume is therefore directly updated.

Energy equation resolution

At this stage of the implicit resolution of the acoustic+dissipative step, specific volume $\vartheta^{\dagger}$, velocity field $\boldsymbol{u}^{\dagger}$ and numerical fluxes $\bar{u}_{\boldsymbol{ij}}^{\dagger}$ and $\bar{p}_{\boldsymbol{ij}}^{\dagger}$ are known. Since mass and volume fractions are not modified by the acoustic+dissipative step, only the new total energy remains unknown. In this step, the evolution equation of the total energy reads

$$\partial_t E + \vartheta \nabla \cdot (p \boldsymbol{u}) = \vartheta \nabla \cdot (\mathsf{T} \boldsymbol{u}) - \vartheta \nabla \cdot \boldsymbol{q}. \tag{27}$$

Because of the term related to the heat flux, the mixture energy cannot be directly updated. A different unknown is used for the implicit resolution of this equation. Since the total energy of the mixture is equal to $E = \varepsilon + \frac{|\boldsymbol{u}|^2}{2}$, where ε is the internal mixture energy (4), the evolution equation of the total energy (27) can be written in terms of the internal mixture energy, namely

$$\partial_t \varepsilon + \vartheta \nabla \cdot \boldsymbol{q} = \vartheta \nabla \cdot (\mathsf{T} \boldsymbol{u}) - \vartheta \nabla \cdot (p \boldsymbol{u}) - \partial_t \frac{|\boldsymbol{u}|^2}{2}. \tag{28}$$

An implicit scheme for this equation is given by

$$\varepsilon_{\boldsymbol{i}}^{\dagger} - \varepsilon_{\boldsymbol{i}}^{n} - \frac{\Delta t}{|\Omega_{\boldsymbol{i}}|}\vartheta_{\boldsymbol{i}}^{n}\nabla_{\boldsymbol{i}}\cdot\boldsymbol{q}^{\dagger} = \frac{\Delta t}{|\Omega_{\boldsymbol{i}}|}\vartheta_{\boldsymbol{i}}^{n}\left(\nabla_{\boldsymbol{i}}\cdot\left(\mathsf{T}^{\dagger}\boldsymbol{u}^{\dagger}\right) - \sum_{\boldsymbol{j}\in v(\boldsymbol{i})}|\Gamma_{\boldsymbol{ij}}|\left(\bar{p}_{\boldsymbol{ij}}^{\dagger}\bar{u}_{\boldsymbol{ij}}^{\dagger}\right)\right) - \frac{1}{2}\left(\left|\boldsymbol{u}_{\boldsymbol{i}}^{\dagger}\right|^{2} - |\boldsymbol{u}_{\boldsymbol{i}}^{n}|^{2}\right). \tag{29}$$

All terms of the right-hand side are already known with the resolution of the velocity-pressure system. This right-hand side is denoted by $SM_{\boldsymbol{i}}^{\dagger}$ in the following.

Like in the explicit scheme, the mixture heat flux is assumed to be given by a Fourier's law $\boldsymbol{q} = -\kappa\boldsymbol{\nabla}T$, with a thermal conductivity of the mixture defined by $\kappa = z\kappa_1 + (1-z)\kappa_2$ and a mixture temperature

$$T = \frac{1}{c_v}\sum_{k=1}^{2} y_k c_{v_k} T_k,$$

where the temperature of the phase k is given by the EOS, namely $T_k(p,\vartheta_k) = \vartheta_k\frac{p+\pi_k}{c_{v_k}(\gamma_k-1)}$. The energy evolution equation can thus be written in terms of the mixture temperature. Indeed, the implicit scheme for the evolution equation of the energy (29) reads

$$\varepsilon(T_{\boldsymbol{i}}^{\dagger},\vartheta_{\boldsymbol{i}}^{\dagger},z_{\boldsymbol{i}}^{\dagger},y_{\boldsymbol{i}}^{\dagger}) - \varepsilon_{\boldsymbol{i}}^{n} - \frac{\Delta t}{|\Omega_{\boldsymbol{i}}|}\vartheta_{\boldsymbol{i}}^{n}\nabla_{\boldsymbol{i}}\cdot\left(\kappa\boldsymbol{\nabla}T^{\dagger}\right) = SM_{\boldsymbol{i}}^{\dagger}. \tag{30}$$

This implicit equation is then solved with a temperature based Newton-Raphson method. When the convergence is reached, a new mixture internal energy can be obtained from (6) and the new total energy is given by

$$E_{\boldsymbol{i}}^{\dagger} = \varepsilon_{\boldsymbol{i}}^{\dagger} + \frac{\left|\boldsymbol{u}_{\boldsymbol{i}}^{\dagger}\right|^{2}}{2}.$$

In conclusion, unlike the inviscid case where there was only a single inversion of a penta-diagonal linear system for the implicit scheme [PGM17, CGK16], here a 9-block linear system needs to be solved for the velocity-pressure system and an iterative process is necessary to find the new mixture energy if the dissipative effects are taken into account.

3.4. Transport step

First of all, since that $\boldsymbol{u}\cdot\boldsymbol{\nabla}\boldsymbol{U} = \nabla\cdot(\boldsymbol{u}\boldsymbol{U}) - \boldsymbol{U}\nabla\cdot\boldsymbol{u}$, then the transport step (14) can be expressed as

$$\partial_t\phi + \nabla\cdot(\boldsymbol{u}\phi) - \phi\nabla\cdot\boldsymbol{u} = 0,$$

with $\phi \in \{\rho, \rho y, \rho\boldsymbol{u}, \rho E, z\}$. An upwind Finite-Volume scheme can be used to solve the transport system like in [CGK16, PGM17, EDKT17]. The transport step is simply approximated by

$$\phi_{\boldsymbol{i}}^{n+1} = \left(1 + \frac{\Delta t}{|\Omega_{\boldsymbol{i}}|}\sum_{\boldsymbol{j}\in v(\boldsymbol{i})}|\Gamma_{\boldsymbol{ij}}|\,\mathfrak{u}_{\boldsymbol{ij}}\right)\phi_{\boldsymbol{i}}^{\dagger} - \frac{\Delta t}{|\Omega_{\boldsymbol{i}}|}\sum_{\boldsymbol{j}\in v(\boldsymbol{i})}|\Gamma_{\boldsymbol{ij}}|\,\mathfrak{u}_{\boldsymbol{ij}}\phi_{\boldsymbol{ij}}^{\dagger}, \tag{31}$$

where $\phi_{\boldsymbol{ij}}^{\dagger}$ is the numerical flux. If the upwind scheme is used, it reads

$$\begin{cases}\phi_{\boldsymbol{ij}}^{\dagger} = \phi_{\boldsymbol{i}}^{\dagger} & \text{if } \mathfrak{u}_{\boldsymbol{ij}} > 0,\\ \phi_{\boldsymbol{ij}}^{\dagger} = \phi_{\boldsymbol{j}}^{\dagger} & \text{otherwise.}\end{cases} \tag{32}$$

The propagation velocity $\mathfrak{u}_{\boldsymbol{ij}}$ of the transport step must be chosen equal to the opposite of the first component of the numerical flux of the acoustic step in order to have a conservative global scheme. Namely, $\mathfrak{u}_{\boldsymbol{ij}} = \bar{u}_{\boldsymbol{ij}}^{n}$ if the first step is solved explicitly or $\mathfrak{u}_{\boldsymbol{ij}} = \bar{u}_{\boldsymbol{ij}}^{\dagger}$ in the implicit case.

The stability condition of this explicit scheme based on material waves reads

$$\max_{\boldsymbol{i}}\left(\frac{\Delta t}{|\Omega_{\boldsymbol{i}}|}\sum_{\boldsymbol{j}\in v(\boldsymbol{i})}|\Gamma_{\boldsymbol{ij}}|\,\mathfrak{u}_{\boldsymbol{ij}}\right) \leq 1. \tag{33}$$

In this work, we are mainly concerned with two-phase flows where the two phases are not initially mixed. For such initial conditions, volume and mass fractions are not modified by the acoustic+dissipative step. However, the upwind scheme for transport step will naturally introduces numerical diffusion, especially on the volume fraction. This will therefore lead to a numerical diffusion of the interface and the introduction of a mixture zone.

A second-order accurate scheme can also be derived for the the transport step with a MUSCL reconstruction [Tor97, GR91]. The accuracy of the scheme is increased by this limitation procedure but the numerical diffusion of the volume fraction is still present.

Several methods are described in the literature to limit numerical diffusion when solving a transport equation. We can cite in particular reconstruction methods such as Volume of Fluid [HN81], Moment of Fluid [AS07, DS08, BHMS13] or Simple Line Interface Calculation [NW76] and the Vofire scheme [DLL07, FK13]. In the anti-diffusive method of Després and Lagoutiere [Lag00, DL99], the flux is chosen as close as possible to the downwind value of the numerical unknown. The resulting scheme is equivalent to the Ultra-Bee limiter [Tor97] in the case of linear advection. This anti-diffusive approach has been extended to the five-equation model (without dissipative effects) by Kokh and Lagoutière [KL10] using a fully explicit Lagrange-Projection scheme. An extension to multi-phase flow has also been done by [FK14]. To completely avoid numerical diffusion of the material interface, another approach is to use Glimm's scheme [Gli65]. This method has been used on two-dimensional Cartesian grid to compute compressible two-phase flows [Jun13, HJ13, BHJ$^+$13]. For more details on numerical methods to ensure the preservation of sharp profiles, let us refer to [DKL16].

To prevent numerical diffusion of the material interface, the anti-diffusive method of [KL10] and Glimm's method proposed by [BHJ$^+$13] are used in this work.

3.4.1. Anti-diffusive scheme

Let us refer to [KL10] for an exhaustive presentation of the construction of the anti-diffusive scheme in the one-dimensional case. A small modification of the anti-diffusive scheme is presented here in the case of slightly deformed curvilinear meshes.

Kokh and Lagoutière [KL10] use a directional splitting to compute the two-dimensional cases. This approach is possible only for Cartesian meshes. However, in the case of liquid ablation considered here, the melting process of the solid part will lead to a deformation of the structured grid. Consequently, a slightly different approach is used herewith the anti-diffusive scheme on slightly deformed curvilinear meshes. The numerical scheme (31) is split into two parts. In the section, the two-index notation (l,m) is used for the sake of clarity. Let ϕ_{x_1} and ϕ_{x_2} be the contributions of direction l and m, respectively, to $\phi_{l,m}^{n+1}$, defined by

$$
\begin{aligned}
(\phi_{x_1})_{l,m}^{n+1} = \phi_{l,m}^{\dagger} &+ 2\frac{\Delta t}{\left|\Omega_{l,m}\right|}\phi_{l,m}^{\dagger}\left(\left|\Gamma_{l+\frac{1}{2},m}\right|\mathfrak{u}_{l+\frac{1}{2},m} - \left|\Gamma_{l-\frac{1}{2},m}\right|\mathfrak{u}_{l-\frac{1}{2},m}\right) \\
&- 2\frac{\Delta t}{\left|\Omega_{l,m}\right|}\left(\left|\Gamma_{l+\frac{1}{2},m}\right|\mathfrak{u}_{l+\frac{1}{2},m}\phi_{l+\frac{1}{2},m}^{\dagger} - \left|\Gamma_{l-\frac{1}{2},m}\right|\mathfrak{u}_{l-\frac{1}{2},m}\phi_{l-\frac{1}{2},m}^{\dagger}\right),
\end{aligned}
$$

and

$$
\begin{aligned}
(\phi_{x_2})_{l,m}^{n+1} = \phi_{l,m}^{\dagger} &+ 2\frac{\Delta t}{\left|\Omega_{l,m}\right|}\phi_{l,m}^{\dagger}\left(\left|\Gamma_{l,m+\frac{1}{2}}\right|\mathfrak{u}_{l,m+\frac{1}{2}} - \left|\Gamma_{l,m-\frac{1}{2}}\right|\mathfrak{u}_{l,m-\frac{1}{2}}\right) \\
&- 2\frac{\Delta t}{\left|\Omega_{l,m}\right|}\left(\left|\Gamma_{l,m+\frac{1}{2}}\right|\mathfrak{u}_{l,m+\frac{1}{2}}\phi_{l,m+\frac{1}{2}}^{\dagger} - \left|\Gamma_{l,m-\frac{1}{2}}\right|\mathfrak{u}_{l,m-\frac{1}{2}}\phi_{l,m-\frac{1}{2}}^{\dagger}\right),
\end{aligned}
$$

so that

$$
\phi_{\boldsymbol{i}}^{n+1} = \frac{1}{2}\left((\phi_{x_1})_{\boldsymbol{i}}^{n+1} + (\phi_{x_2})_{\boldsymbol{i}}^{n+1}\right).
$$

The anti-diffusive method given by Kokh and Lagoutière is used for each mesh direction to compute the numerical fluxes $\phi^\dagger_{l\pm\frac{1}{2},m}$ and $\phi^\dagger_{l,m\pm\frac{1}{2}}$. For direction l, the upwind value according to the sign of $\mathfrak{u}_{l+\frac{1}{2},m}$ is chosen for $\rho_1^\dagger, \rho_2^\dagger, (\rho_1\varepsilon_1)^\dagger$ and $(\rho_2\varepsilon_2)^\dagger$. For the flux of the volume fraction evolution equation $z^\dagger_{l+\frac{1}{2},m}$, the idea is to find the interval $I_{l+\frac{1}{2},m}$ which provides stability and consistency for the volume fraction and then to choose "the most downwind" possible value. Following Kokh and Lagoutière method, we want to make sure the flux $z^\dagger_{l+\frac{1}{2},m}$ belongs to the interval $\left[m_{l+\frac{1}{2},m}, M_{l+\frac{1}{2},m}\right]$ to ensure consistency, where

$$m_{l+\frac{1}{2},m} = \min(z^n_{l,m}, z^n_{l+1,m}), \tag{34}$$

$$M_{l+\frac{1}{2},m} = \max(z^n_{l,m}, z^n_{l+1,m}). \tag{35}$$

Suppose that $\mathfrak{u}_{l-\frac{1}{2},m} > 0$ and $\mathfrak{u}_{l+\frac{1}{2},m} > 0$. To ensure the stability of the solution, the flux $z_{l+\frac{1}{2},m}$ must belong to the interval $\left[a_{l+\frac{1}{2},m}, A_{l+\frac{1}{2},m}\right]$, where

$$a_{l+\frac{1}{2},m} = z^n_{l,m} + \frac{M_{l-\frac{1}{2},m} - z^n_{l,m}}{\left|\Gamma_{l+\frac{1}{2},m}\right| \mathfrak{u}_{l+\frac{1}{2},m}} \left(\left|\Gamma_{l-\frac{1}{2},m}\right| \mathfrak{u}_{l-\frac{1}{2},m} - \frac{\left|\Omega_{l,m}\right|}{2\Delta t} \right), \tag{36}$$

$$A_{l+\frac{1}{2},m} = z^n_{l,m} + \frac{m_{l+\frac{1}{2},m} - z^n_{l,m}}{\left|\Gamma_{l+\frac{1}{2},m}\right| \mathfrak{u}_{l+\frac{1}{2},m}} \left(\left|\Gamma_{l-\frac{1}{2},m}\right| \mathfrak{u}_{l-\frac{1}{2},m} - \frac{\left|\Omega_{l,m}\right|}{2\Delta t} \right). \tag{37}$$

The other cases depending on the sign of the velocity can be calculated in a similar way. After determining the different intervals, the flux value $z^\dagger_{l+\frac{1}{2},m}$ is computed as in the one-dimensional case, see [KL10] for details.

This approach based on a decomposition of the solution according to the mesh directions is only valid for slightly deformed Cartesian meshes. The use of a genuinely two-dimensional scheme to prevent diffusion of the material interface would overcome this limitation.

3.4.2. Glimm's method

The second approach to solve the transport step is not based on a Finite Volume scheme but on Glimm's random choice method [Gli65, Col82, HJ13].

A pseudo-random sequence $\omega^n \in [0, 1[$ is considered. In the one-dimensional case, the pseudo-random averaging associated to this choice is given by

$$\phi_i^{n+1} = \begin{cases} \phi^\dagger_{i-1} & \text{if } \omega^n < \frac{\Delta t}{\Delta x_i}\mathfrak{u}_{i-\frac{1}{2}}, \\ \phi^\dagger_{i} & \text{if } \frac{\Delta t}{\Delta x_i}\mathfrak{u}_{i-\frac{1}{2}} \leq \omega^n \leq 1 + \frac{\Delta t}{\Delta x_i}\mathfrak{u}_{i+\frac{1}{2}}, \\ \phi^\dagger_{i+1} & \text{if } \omega^n > 1 + \frac{\Delta t}{\Delta x_i}\mathfrak{u}_{i+\frac{1}{2}}. \end{cases} \tag{38}$$

Note that the pseudo-random number ω^n does not depend on the considered cell mesh but only on the time iteration. The (5,3) van der Corput sequence is used to compute the pseudo-random sequence [Col82, HJ13]. A schematic representation of the pseudo-random averaging is provided in Fig. 6.

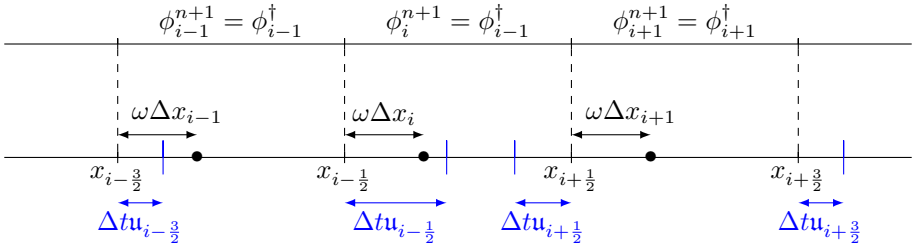

Figure 6: Computation of the solution for the cells $i-1$, i and $i+1$ with Glimm's pseudo-random averaging.

If this random averaging method is applied in the whole computational domain, Jung [Jun13, BHJ$^+$13] shows that the method introduces instabilities for strong shocks. Glimm's method is therefore used only at the material interfaces between

the two phases. In pure phase areas, the upwind scheme is used. In the following and for the sake of simplicity, this hybrid method between the upwind scheme for pure zones and the random Glimm's method for mixing zones is simply denoted by Glimm's method. In the two-dimensional case, a directional splitting is used. This method can therefore only be used on Cartesian meshes in 2D configurations.

3.5. Numerical procedure with moving grids

The main goal of this paper is to develop numerical tools in order to handle complex multi-physics configurations and especially the melting of a solid domain. The interface between the solid and the fluid domains, *i.e.* the melting front, is therefore going to move over time. In this section, the discretization of the governing equations for both domains over a moving domain is described. An Arbitrary Lagrangian Eulerian approach, equivalent to a space-time Finite Volume method, is used here.

In this work, curvilinear grids are considered and the node displacement is done on the mesh lines. In order to simplify the computation of mass and energy balances, conforming mesh for the fluid and solid domains are used.

3.5.1. Fluid domain

For the fluid area, the two-phase flow model with dissipative effects (2) can be written in compact form

$$\partial_t \boldsymbol{U} + \nabla \cdot \boldsymbol{F} + \boldsymbol{H}\boldsymbol{\nabla} z = 0, \tag{39}$$

with $\boldsymbol{U} = (\rho, \rho y, \rho \boldsymbol{u}, \rho E, z)^T$, $\boldsymbol{F} = (\rho \boldsymbol{u}, \rho y \boldsymbol{u}, \rho \boldsymbol{u} \otimes \boldsymbol{u} - \mathsf{S}, \rho E \boldsymbol{u} - \mathsf{S}\boldsymbol{u} + \boldsymbol{q}, 0)^T$ and the vector $\boldsymbol{H} = (0, 0, 0, 0, \boldsymbol{u})^T$. The stress tensor S is given by $\mathsf{S} = \mathsf{T} - p\mathsf{I_d}$ for the sake of clarity.

The previous system (39) is integrated over a control volume $\omega(t)$ moving at the velocity denoted by $\boldsymbol{w}$. It reads

$$\int_{\omega(t)} \left(\partial_t \boldsymbol{U} + \nabla \cdot \boldsymbol{F} + \boldsymbol{H}\boldsymbol{\nabla} z\right) \mathrm{d}v = 0.$$

Noticing that the flux $\boldsymbol{F}$ can be expressed as $\boldsymbol{F} = \boldsymbol{u}\boldsymbol{U} + \boldsymbol{G}^0$ where $\boldsymbol{G}^0 = (0, 0, -\mathsf{S}, -\mathsf{S}\boldsymbol{u} + \boldsymbol{q}, -\boldsymbol{u}z)^T$, we have

$$\int_{\omega(t)} \left(\partial_t \boldsymbol{U} + \boldsymbol{U}\nabla \cdot \boldsymbol{u} + \nabla \cdot \boldsymbol{G}^0 + \boldsymbol{H}\boldsymbol{\nabla} z + \boldsymbol{u} \cdot \boldsymbol{\nabla}\boldsymbol{U}\right) \mathrm{d}v = 0. \tag{40}$$

When moving grids are considered, Geometric Conservation Law (GCL) has to be satisfied at the discrete level in order to ensure the preservation of constant states while the mesh is moving [LF96]. At the continuous level, the GCL reads

$$\frac{\mathrm{d}}{\mathrm{d}t}\left(|\omega(t)|\right) - \int_{\partial\omega(t)} \boldsymbol{w} \cdot \mathbf{n}\, \mathrm{d}\sigma = 0, \tag{41}$$

where the boundary of the control volume is denoted by $\partial\omega(t)$ and $\boldsymbol{n}$ is the unit normal pointing outward.

Following the case where the mesh is not moving, see section 3.2, an operator splitting strategy is used to approximated the five-equation model (2) on a moving mesh while preserving the Geometric Conservation Law. To do so, the system and the GCL are split into two parts: an acoustic+dissipative step

$$\begin{cases} \displaystyle\int_{\omega(t)} \left(\partial_t \boldsymbol{U} + \boldsymbol{U}\nabla \cdot \boldsymbol{u} + \nabla \cdot \boldsymbol{G}^0 + \boldsymbol{H}\boldsymbol{\nabla} z\right) \mathrm{d}v = 0, \\ \displaystyle\frac{\mathrm{d}}{\mathrm{d}t}\left(|\omega(t)|\right) = 0, \end{cases} \tag{42}$$

and a transport step

$$\begin{cases} \displaystyle\int_{\omega(t)} \left(\partial_t \boldsymbol{U} + \boldsymbol{u} \cdot \boldsymbol{\nabla}\boldsymbol{U}\right) \mathrm{d}v = 0, \\ \displaystyle\frac{\mathrm{d}}{\mathrm{d}t}\left(|\omega(t)|\right) - \int_{\partial\omega(t)} \boldsymbol{w} \cdot \mathbf{n}\, \mathrm{d}\sigma = 0. \end{cases} \tag{43}$$

The acoustic+dissipative step is solved on a fixed mesh, *i.e.* set $\omega(t) = \omega(t^n) = \omega^n$. The explicit scheme is described in sections 3.1 and 3.3.1 while the implicit treatment is given in sections 3.1 and 3.3.2.

For the transport step (43), note that it can still be expressed as

$$\int_{\omega(t)} \left(\partial_t \phi + \nabla \cdot (\boldsymbol{u}\phi) - \phi \nabla \cdot \boldsymbol{u}\right) \mathrm{d}v = 0, \tag{44}$$

where ϕ can be ρ, ρy, $\rho \boldsymbol{u}$, ρE or z.

For the first term of (44), we use the Reynolds transport formula to get

$$\int_{\omega(t)} \frac{\partial \phi}{\partial t} \mathrm{d}v = \frac{\mathrm{d}}{\mathrm{d}t} \int_{\omega(t)} \phi \, \mathrm{d}v - \int_{\partial\omega(t)} \phi \boldsymbol{w} \cdot \mathbf{n} \, \mathrm{d}\sigma. \tag{45}$$

Then transport system (44) can be rewritten as

$$\frac{\mathrm{d}}{\mathrm{d}t} \int_{\omega(t)} \phi \, \mathrm{d}v - \int_{\partial\omega(t)} \phi \boldsymbol{w} \cdot \mathbf{n} \, \mathrm{d}\sigma + \int_{\omega(t)} \left(\nabla \cdot (\boldsymbol{u}\phi) - \phi \nabla \cdot \boldsymbol{u}\right) \mathrm{d}v = 0,$$

where $\phi \in \{\rho, \rho y, \rho \boldsymbol{u}, \rho E, z\}$, or also

$$\frac{\mathrm{d}}{\mathrm{d}t} \int_{\omega(t)} \phi \, \mathrm{d}v + \int_{\partial\omega(t)} \phi(\boldsymbol{u} - \boldsymbol{w}) \cdot \mathbf{n} \, \mathrm{d}\sigma - \int_{\omega(t)} \phi \nabla \cdot \boldsymbol{u} \, \mathrm{d}v = 0.$$

For the cell $\Omega_{\boldsymbol{i}}(t)$, the mean value theorem gives

$$\frac{\mathrm{d}}{\mathrm{d}t} \left(|\Omega_{\boldsymbol{i}}| \, \phi_{\boldsymbol{i}}\right) + \int_{\partial\Omega_{\boldsymbol{i}}(t)} \phi(\boldsymbol{u} - \boldsymbol{w}) \cdot \mathbf{n} \, \mathrm{d}\sigma - \phi_{\boldsymbol{i}} \int_{\partial\Omega_{\boldsymbol{i}}(t)} \boldsymbol{u} \cdot \mathbf{n} \, \mathrm{d}\sigma = 0.$$

Note that the Geometric Conservation Law is satisfied with this formulation. The explicit numerical scheme used for the transport step if the the mesh is moving at the velocity $\boldsymbol{w}$ then is given by

$$\left|\Omega_{\boldsymbol{i}}^{n+1}\right| \phi_{\boldsymbol{i}}^{n+1} = |\Omega_{\boldsymbol{i}}^{n}| \, \phi_{\boldsymbol{i}}^{\dagger} - \Delta t \sum_{\boldsymbol{j} \in v(\boldsymbol{i})} |\Gamma_{\boldsymbol{ij}}| \, \phi_{\boldsymbol{ij}}^{\dagger} (\mathfrak{u}_{\boldsymbol{ij}} - \bar{w}_{\boldsymbol{ij}}) + \Delta t \phi_{\boldsymbol{i}}^{\dagger} \sum_{\boldsymbol{j} \in v(\boldsymbol{i})} |\Gamma_{\boldsymbol{ij}}| \, \mathfrak{u}_{\boldsymbol{ij}}, \tag{46}$$

where $\bar{w}_{\boldsymbol{ij}}$ is the material velocity of the face $\Gamma_{\boldsymbol{ij}}$. If the mesh is not moving, this material velocity is given by the Riemann solver of the first step, in order to have a conservative discretization for the global scheme (see section 3.4). We keep this choice of material speed on the face when the mesh moves. The numerical flux $\phi_{\boldsymbol{ij}}^{\dagger}$ depends on the choice of the scheme in the transport step. In the case of the upwind scheme, the flux is given by

$$\begin{cases} \phi_{\boldsymbol{ij}}^{\dagger} = \phi_{\boldsymbol{i}}^{\dagger} & \text{if } \bar{u}_{\boldsymbol{ij}} - \bar{w}_{\boldsymbol{ij}} > 0, \\ \phi_{\boldsymbol{ij}}^{\dagger} = \phi_{\boldsymbol{j}}^{\dagger} & \text{otherwise.} \end{cases}$$

In the case of the anti-diffusive scheme, the construction of the flux is analog to the one presented in section 3.4.1.

3.5.2. Solid domain

The heat equation inside the solid can also be integrate over a moving control volume $\omega_s(t)$

$$\int_{\omega_s(t)} \partial_t(\rho_s \varepsilon_s) \, \mathrm{d}v = \int_{\omega_s(t)} \nabla \cdot (\kappa_s \boldsymbol{\nabla} T_s) \, \mathrm{d}v.$$

Using once again the Reynolds transport formula and the divergence theorem, we get

$$\frac{\mathrm{d}}{\mathrm{d}t} \int_{\omega_s(t)} \rho_s \varepsilon_s \, \mathrm{d}v - \int_{\partial\omega(t)} \rho_s \varepsilon_s \boldsymbol{w} \cdot \mathbf{n} \, \mathrm{d}\sigma = \int_{\partial\omega(t)} \kappa_s \boldsymbol{\nabla} T_s \cdot \mathbf{n} \, \mathrm{d}\sigma.$$

The numerical scheme is then given by

$$\left|\Omega_{\boldsymbol{i}}^{n+1}\right| \rho_{\boldsymbol{i}}^{n+1} \varepsilon_{\boldsymbol{i}}^{n+1} = |\Omega_{\boldsymbol{i}}^{n}| \, \rho_{\boldsymbol{i}}^{n} \varepsilon_{\boldsymbol{i}}^{n} + \Delta t \sum_{\boldsymbol{j} \in v(\boldsymbol{i})} |\Gamma_{\boldsymbol{ij}}| \, (\rho\varepsilon)_{\boldsymbol{ij}}^{n} \bar{w}_{\boldsymbol{ij}} - \Delta t \nabla_{\boldsymbol{i}} \cdot \boldsymbol{q}_s^{n+1}. \tag{47}$$

An implicit scheme is still used for the diffusive part. An explicit upwind scheme is used for the term related to (slow) mesh movement due to the ablation of the solid domain. Namely, it reads

$$\begin{cases} (\rho\varepsilon)_{\boldsymbol{ij}}^{n} = (\rho\varepsilon)_{\boldsymbol{i}}^{n} & \text{if } \bar{w}_{\boldsymbol{ij}} < 0, \\ (\rho\varepsilon)_{\boldsymbol{ij}}^{n} = (\rho\varepsilon)_{\boldsymbol{j}}^{n} & \text{otherwise.} \end{cases}$$

4. Fluid-Solid coupling algorithm

After the description of the governing equations and the numerical procedure, a coupling algorithm between the fluid and solid domains in order to simulate the melting process of a metallic material can now be defined. The following coupling algorithm is proposed

Step 1. Fluid and solid domains are initialized everywhere. Note that the location of the fluid-solid interface is known.

Step 2. The mass flux $\dot{m}$ at the interface between liquid and solid domains is computed from the energy balance (10).

Step 3. From mass balance (7) and from mass flux $\dot{m}$, the interface velocity w_{itf} (8) and the injection velocity $\boldsymbol{u}_f$ (9) are computed.

Step 4. Time steps for the fluid and solid domains are computed by taking into account the interface velocity. The overall time step will be the minimum of the time steps for the two domains.

Step 5. The interface is moved to its new position. The meshes of the two domains are reconstructed on both sides of the interface.

Step 6. The unsteady solution in the fluid domain is calculated from the solution of the previous coupling time step: first, the acoustic+dissipative step is solved on the fluid mesh at time t^n, see section 3.3, then transport step (46) is solved on the new mesh as described in section 3.5.1. A Dirichlet condition to ensure the melting temperature T_w is applied on the wall. The velocity of the fluid at the interface between the fluid and the solid is given by the injection velocity $\boldsymbol{u}_f$ (9).

Step 7. The unsteady solution of the heat equation (1) inside the solid domain is computed from the solution at the previous coupling time step as described in section 3.5.2. A Dirichlet boundary condition at the melting temperature T_w is also imposed at the solid fluid interface.

Step 8. The solution of the current coupling time step is determined: the position of the wall and fields for both fluid and solid domains are known. Go to the next coupling time step by starting at Step 2 of the algorithm.

In the case of multiphase ablation studied here, one can note that the computation of the fluid domain, Step 6, and the solid one, Step 7, can be solved at the same time in the algorithm proposed above.

5. Numerical validation

The main objective of this section is to validate the numerical scheme previously described to take into account the diffusion terms in the two-phase flows model. First of all, the choice of the mixture temperature based on the internal energy form is discussed. In order to do so, a two-phase flow shock tube test case is used. A classical single-phase Couette-type flow test case is next considered as a validation of the discretization of the dissipation terms. The impact of the neglected terms in the pressure evolution equation (22) for the implicit formulation is also discussed with this test case. The discretization of the dissipation terms for a mixture of two fluids and the implicit formulation of the equation on energy is then validated using a two-phase Couette-type flow. For the last test case, the melting of an aluminium solid block by a lid-driven cavity filled with air is considered. The three material phases are involved in this test case. The liquid phase is not initially present inside the fluid domain, but the ablation of the solid part creates a molten layer between the gas and the wall. The ALE formulation of the numerical schemes presented before is needed since the interface between the fluid and the solid domain is explicit tracked and therefore the whole mesh is moving.

In the sequel, the fully explicit-scheme for the five-equation system with dissipative effects inside the fluid domain is denoted by EXEX, while the implicit-explicit splitting scheme is denoted by IMEX.

5.1. Two-phase flow shock-tube test: mixture temperature choice

To illustrate the choice of the mixture temperature, a classical one-dimensional shock tube problem between water and air is considered [PGM17]. The stiffened gas equation of state is used for the liquid while the air is modeled by a perfect gas law. At the initial time, the interface between the two fluids at rest is at $x = 0.7$ m. Let us recall that the initial characteristics of water and air are given by

$$\begin{cases} (\rho, p, u, \gamma, \pi) = \left(1000 \text{ kg.m}^{-3}, 10^9 \text{ Pa}, 0 \text{ m.s}^{-1}, 4.4, 6 \times 10^8 \text{ Pa}\right) & \text{for } 0\text{m} \leq x < 0.7\text{m}, \\ (\rho, p, u, \gamma, \pi) = \left(50 \text{ kg.m}^{-3}, 10^5 \text{ Pa}, 0 \text{ m.s}^{-1}, 1.4, 0 \text{ Pa}\right) & \text{for } 0.7\text{m} \leq x \leq 1\text{m}. \end{cases}$$

In order to compute the temperature, the heat capacity at constant volume c_v of each phase needs to be known. For the liquid phase, $c_v = 4180$ J.kg^{-1}.K^{-1} and the heat capacity for the gas phase is equal to $c_v = 1000$ J.kg^{-1}.K^{-1}. A 1000 cells mesh is used for the computation and constant state boundary conditions are applied on each side on the computational domain. The second-order explicit scheme is used here, and the time step is given by the two stability conditions (18) and (33) with a CFL number equals to 0.2.

In this first test case, dissipative terms are not taken into account. The temperature is only a post-processed quantity. The choice of the definition of the mixture temperature will therefore not influence the computation of the other physical variables. Starting from the definition of the internal mixture energy, a mixture temperature can be derived

$$T_\varepsilon(p, \vartheta, z, y) = \frac{1}{c_v(y)} \sum_{k=1}^{2} y_k c_{v_k} T_k. \tag{48}$$

This mixture temperature based on the internal energy is a convex combination of the temperature of each phase $T_k(p, \vartheta_k) = \vartheta_k \frac{p+\pi_k}{c_{v_k}(\gamma_k - 1)}$. However, it is also possible to define a mixture temperature by considering the mixture entropy for two stiffened gases

$$s = c_v(y) \ln\left((p + \pi(z))\vartheta^{\gamma(z)}\right).$$

Indeed, following Gibbs equation $Tds = d\varepsilon + pd\vartheta + fdz + gdy$, we can find that the temperature is equal to $T = \left(\frac{\partial s}{\partial \varepsilon}\big|_{\vartheta,z,y}\right)^{-1}$. The temperature T_s related to the entropy is thus given by

$$T_s(p, \vartheta, z, y) = \vartheta \frac{p + \pi(z)}{c_v(y)(\gamma(z) - 1)}. \tag{49}$$

Note that, if the two reference pressures π_1 and π_2 are equal, the two temperature definitions coincide. This is no longer true if the reference pressures are different as in the case of an air-water mixture.

The two mixture temperatures defined by (48) and (49) computed with the second-order EXEX scheme are plotted in Fig. 7. One can see that the two temperature definitions give the same result very close to the exact solution in pure fluids areas. However, a temperature peak appears in the mixture zone with the entropy related temperature. Moreover, this overestimation of the temperature does not disappear if the mesh is refined as it is shown in Fig. 8, where a mesh ten times finer has been used. Therefore, the mixture temperature computed with formula (48) derived from the form of the internal mixture energy will only be considered in the following.

5.2. Single phase Couette flow

For the sake of readability, the 2D space variable will be denoted by $\boldsymbol{x} = (x, y)^T$ and the velocity vector by $\boldsymbol{u} = (u, v)^T$ in the next sections 5.2 and 5.3.

In this test case, a laminar flow between two horizontal infinite plates is considered. The two surfaces are separated by a distance $y_e - y_w$. The top plate is moving with a constant velocity denoted by u_e, whereas the bottom one is motionless. In addition, the upper plate is heated to the temperature T_e and the lower surface to temperature T_w with $T_e > T_w$. The test-case geometry is described in Fig. 9.

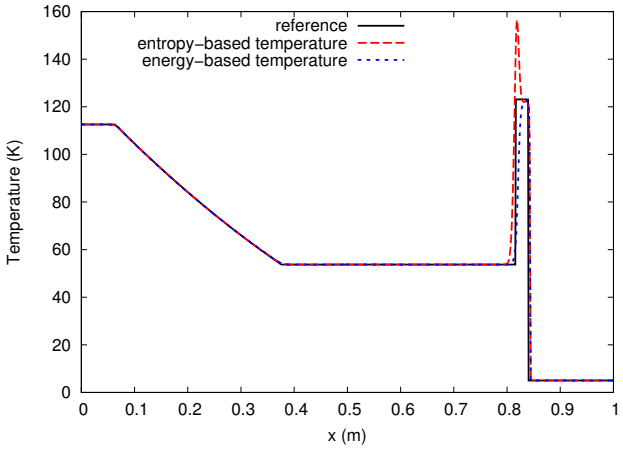

Figure 7: Two-phase flow shock-tube test with a 1000 cells mesh: comparison between the internal energy-based and the entropy-based temperatures.

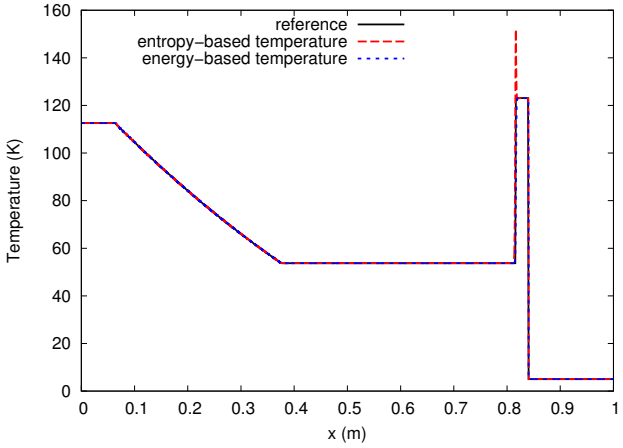

Figure 8: Two-phase flow shock-tube test with a 10 000 cells mesh: comparison between the internal energy-based and the entropy-based temperatures on a mesh ten times finer.

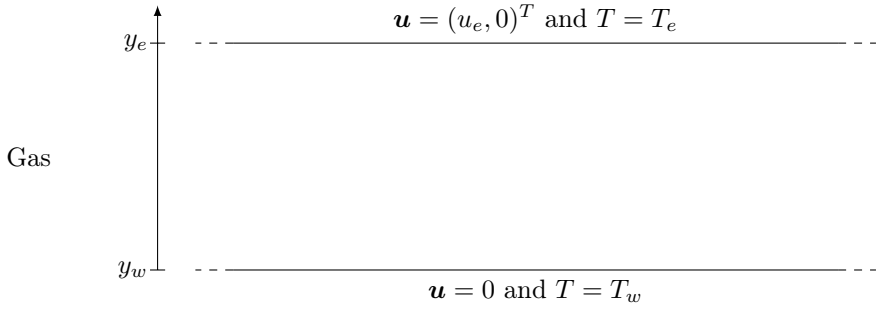

Figure 9: Single phase Couette flow: geometry description and boundary conditions.

The exact resolution of this problem is detailed in Appendix A.1. The velocity profile is given by

$$u(y) = u_e \frac{y - y_w}{y_e - y_w}, \tag{50}$$

whereas the temperature profile is given by

$$T(y) = T_w + \left(T_e - T_w + \frac{\mu u_e^2}{2\kappa} \left(1 - \frac{y - y_w}{y_e - y_w} \right) \right) \frac{y - y_w}{y_e - y_w}, \tag{51}$$

where μ and κ are the viscosity and thermal conductivity of the fluid. They are assumed to be constant here. Previous formulation can be simplified with the introduction of the dimensionless length $\tilde{y} = \frac{y - y_w}{y_e - y_w}$ and the dimensionless temperature $\tilde{T} = \frac{T - T_w}{\Delta T}$ where $\Delta T = T_e - T_w$. Temperature profile can be rewritten as

$$\tilde{T}(\tilde{y}) = \left(1 + \frac{1}{2} PrEc\,(1 - \tilde{y}) \right) \tilde{y}.$$

with the dimensionless number of Prandtl $Pr = \frac{\mu c_p}{\kappa}$ and Eckert $Ec = \frac{u_e^2}{c_p \Delta T}$. One can notice that for configurations such as $PrEc$ >2, the maximum temperature is reached within the domain.

For this test case, the plate located in $y_w = 0$ m is heated to the temperature $T_w = 280$ K. For the upper plate located in $y_e = 0.2$ m, the following boundary conditions are used: $T_e = 330$ K and $u_e = 10$ m.s^{-1}. The fluid between the two plates is assimilated to a perfect gas with $\gamma = 1.4$ and a Prandtl number equal to 0.72. The gas is initialized at atmospheric pressure and with an initial density equals to $\rho_{ini} = 1$ kg.m^{-3}. The viscosity of the fluid is set to $\mu = 1$ Pa.s. By imposing $PrEc = 5$, the other properties of the gas can be obtained, namely $\kappa = 0.4$ W.m^{-1}.K^{-1}, $c_p = 0.288$ J.kg^{-1}.K^{-1} and $c_v = 0.206$ J.kg^{-1}.K^{-1}.

The Courant number used for this test case is equal to 0.8. A 25 cells mesh have been used in the y-direction. To find the steady solution of the problem, an unsteady process is used and the solution will be obtained at the end of the convergence in time. To characterize this steady state, the residual r is computed by comparing the L^2-norm of the difference of the vectors of the conservative unknowns at the pseudo-times $n+1$ and n. This difference is divided by the norm of the conservative vector at the initial time t^0. Thus, the residual is given by

$$r = \frac{\|\boldsymbol{U}^{n+1} - \boldsymbol{U}^n\|_{L^2}}{\|\boldsymbol{U}^0\|_{L^2}},$$

where $\boldsymbol{U} = (\rho, \rho y, \rho \boldsymbol{u}, \rho E, z)^T$. The steady solution is assumed to be reached when the residual is below a convergence criterion. For this simulation, the convergence criterion is set to 10^{-10}.

In figure 10, the temperature and velocity profiles obtained with the fully explicit and implicit-explicit formulations of the numerical scheme have been plotted. One can see that the two curves coincide and are very close to the theoretical solution. This simple test case allows us to validate the discretization of the viscous terms in a single phase flow. The excellent agreement between the EXEX and IMEX schemes shows that the contribution of the heat flow term in pressure evolution equation (22) is small.

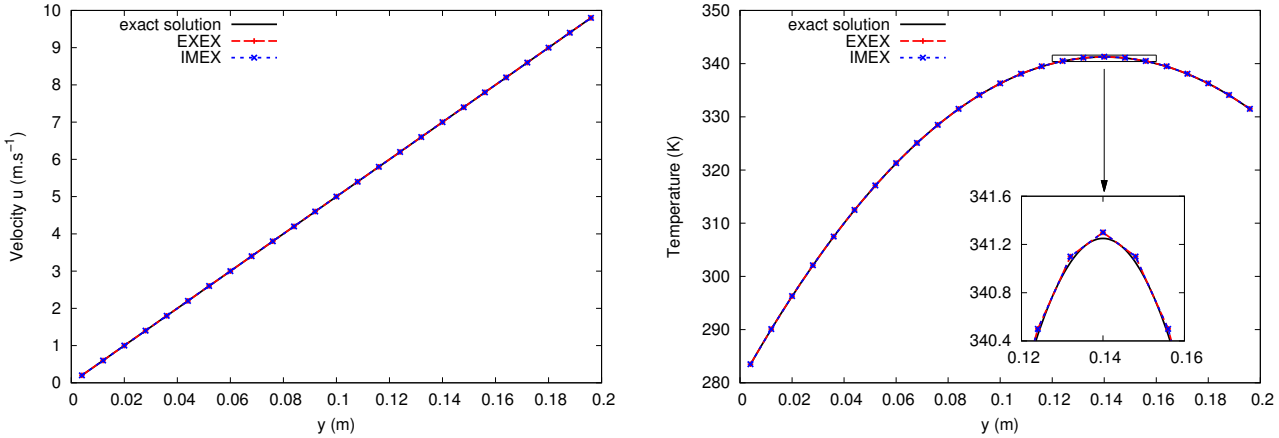

(a) Velocity profiles (b) Temperature profiles

Figure 10: Single phase Couette flow: velocity and temperature profiles obtained with EXEX and IMEX schemes on a 25 cells mesh.

Table 1 gives L^2-norm of the relative error between the numerical temperature obtained with IMEX scheme and the exact solution (51). From this table, one can verify that the discretization of the dissipative terms is second-order accurate.

Cells number	Relative error	Convergence order
10	9.57×10^{-4}	2.00
25	1.53×10^{-4}	2.00
50	3.83×10^{-5}	2.00
100	9.57×10^{-6}	

Table 1: Single phase Couette flow: relative error in L^2-norm and convergence order for the temperature profile obtained with the IMEX scheme.

Remark 4
With the numerical scheme based on a splitting strategy described previously, it is possible to show that, at convergence, the steady solution of the overall scheme still depends on the time step. However, the impact of this dependence have not been noticed in our numerical tests.

5.3. Two-phase Couette flow

As in the previous test case, a physical domain delimited by two infinite horizontal plates separated by a distance $y_e - y_w$ is considered. The upper wall moves at constant speed u_e while the lower wall is fixed. In addition, the upper wall is heated to the temperature T_e and the lower wall to the temperature T_w with $T_e > T_w$. For this test case, a two-phase flow between the two surfaces is considered. The position of the interface between the two fluids is located in $y = y_0$. During the transient phase, the material interface will move. The geometry of the test case is described in Fig 11.

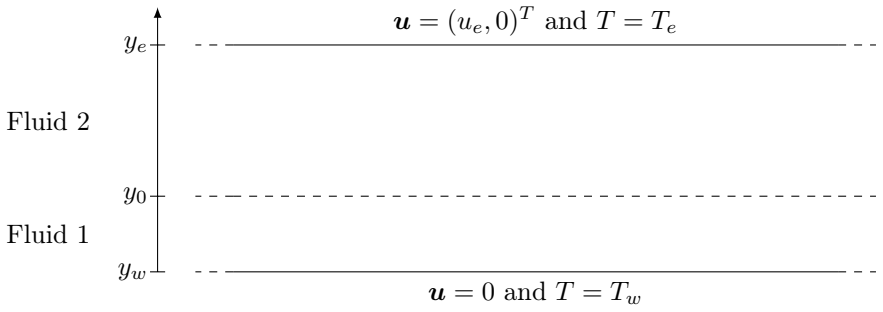

Figure 11: Two-phase Couette flow: geometry description and boundary conditions.

The analytical study of this problem is detailed in Appendix A. Velocity, temperature and pressure profiles can be expressed as a function of the position of the interface y_0 between the two fluids. Indeed, by denoting $L_1 = y_0 - y_w$ and $L_2 = y_e - y_0$, the velocity profile is given by

$$u(y) = \begin{cases} u_0 \dfrac{y - y_w}{L_1} & y_w < y < y_0, \\ u_0 + (u_e - u_0)\dfrac{y - y_0}{L_2} & y_0 < y < y_e, \end{cases} \tag{52}$$

where u_0 is the velocity at the material interface

$$u_0 = \frac{\frac{\mu_2}{L_2} u_e}{\frac{\mu_1}{L_1} + \frac{\mu_2}{L_2}}.$$

The temperature profile is parabolic in each zone. It is given by

$$T(y) = \begin{cases} -\dfrac{\mu_1 u_0^2}{2\kappa_1}\left(\dfrac{y - y_w}{L_1}\right)^2 + \left(T_0 - T_w + \dfrac{\mu_1 u_0^2}{2\kappa_1}\right)\dfrac{y - y_w}{L_1} + T_w & y_w < y < y_0, \\ -\dfrac{\mu_2 (u_e - u_0)^2}{2\kappa_2}\left(\dfrac{y - y_0}{L_2}\right)^2 + \left(T_e - T_0 + \dfrac{\mu_2 (u_e - u_0)^2}{2\kappa_2}\right)\dfrac{y - y_0}{L_2} + T_0 & y_0 < y < y_e, \end{cases} \tag{53}$$

where T_0 is the temperature at the interface between the two phases

$$T_0 = \frac{1}{\frac{\kappa_1}{L_1} + \frac{\kappa_2}{L_2}}\left(\frac{\kappa_1}{L_1} T_w + \frac{\kappa_2}{L_2} T_e + \frac{\mu_1 u_0^2}{2L_1} + \frac{\mu_2 (u_e - u_0)^2}{2L_2}\right).$$

The pressure is constant in the entire domain and its value is given by

$$P = \frac{M_{ini} - \frac{\pi_1 I_1}{(\gamma_1 - 1) c_{v_1}} - \frac{\pi_2 I_2}{(\gamma_2 - 1) c_{v_2}}}{\frac{I_1}{(\gamma_1 - 1) c_{v_1}} + \frac{I_2}{(\gamma_2 - 1) c_{v_2}}}, \tag{54}$$

where M_{ini} is the initial mass, $I_1 = \displaystyle\int_{y_w}^{y_0} \frac{\mathrm{d}y}{T(y)}$ and $I_2 = \displaystyle\int_{y_0}^{y_e} \frac{\mathrm{d}y}{T(y)}$ are the integrals of the inverse of the temperature in both zones.

Finally, velocity (52) and temperature (53) profiles and the value of the pressure P (54) are given as functions of the position of the fluid interface y_0. To find the location of the material interface, the mass conservation applied to the first fluid can be used. It reads

$$(P(y_0) + \pi_1) I_1(y_0) = M^1_{ini}(\gamma_1 - 1) c_{v_1},$$

where M^1_{ini} is the initial mass of the fluid phase 1. This non-linear equation can be solved in order to find the location of the interface y_0 between the two phases. In this work, a simpler approach is used to find the interface position y_0. In order to validate this test case, a reference computation is done (see below) and the location of the material interface in the steady state computed numerically is used. The temperature and velocity profiles can then be obtained. The value of the theoretical pressure is computed from the relation (54) and compared with the value of the pressure obtained by the numerical scheme.

For this two-phase flow simulation, the lower surface located in $y_w = 0$ m is supposed to be heated to the temperature $T_w = 310$ K. For the upper plate located in $y_e = 0.2$ m, the following boundary condition are applied: $T_e = 330$ K and $u_e = 10$ m.s^{-1}. Fluid 1, located in the lower part of the domain, is supposed to be a liquid modeled by stiffened gas equation of state, while fluid 2 is a perfect gas. Parameters for both fluid phases are given in the table 2.

	fluid 1	fluid 2
viscosity μ	10	1
thermal conductivity κ	10	1.376
heat capacity c_v	3.229	0.708
adiabatic exponent γ	3	1.4
reference pressure π	10^5	0

Table 2: Two-phase Couette flow: parameters for each phase.

First, the material interface is originally located in the middle of the domain, *i.e.* $y_{0,ini} = 0.1$ m. Initial densities are equal to $\rho_{1,ini} = 25$ kg.m^{-3} for the liquid and $\rho_{2,ini} = 1.7085$ kg.m^{-3} for the gas. The initial mass in the domain is therefore given by

$$M_{ini} = \rho_{1,ini}(y_{0,ini} - y_w) + \rho_{2,ini}(y_e - y_{0,ini}) = 2.67085 \text{ kg}.$$

The pressure value, velocity and temperature profiles have been expressed as functions of the interface position y_0 between the two fluids. A reference value for the location of the interface needs to be find. In order to do this, the Glimm's method, which does not create a mixture zone, is used in the transport step of the splitting scheme. Let us recall that this method is actually an hybrid method with the use of the upwind scheme in pure fluid zones and the Glimm's random choice method at the interface (see section 3.4.2). A very fine mesh with 4000 cells is used and the numerical position of the material interface in found to be located in $y_0 = 0.050194$ m in the steady state. From this reference value, the theoretical temperature, velocity and pressure profiles can be derived.

As for the single-phase version of the Couette-type flow, the steady solution is computed with a convergence criterion equal to 10^{-10}.

First of all, explicit and implicit formulations of the acoustic step with the dissipative terms are compared. Velocity and temperature profiles obtained by the EXEX and IMEX schemes are plotted in Fig. 12. In the transport step, the upwind scheme has been used. The impact on the solution of the transport scheme choice will be highlighted in the following. The solutions computed with the implicit and explicit formulations are very close, which enables the validation the implicit discretization proposed for the acoustic step. The comparison of the iterations needed to converge to the steady state shows the benefit of the IMEX scheme. Indeed, the implicit formulation of the first step of the scheme requires only 236 iterations

while 2 108 056 iterations are necessary with the fully explicit scheme. In the following, IMEX scheme will only be used and the impact of the transport scheme on the solution will be discussed.

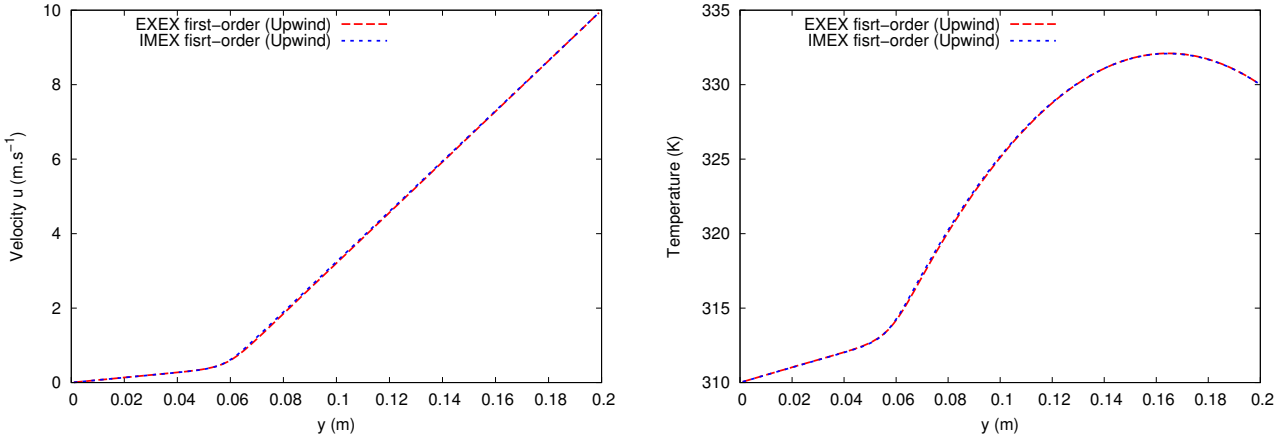

(a) Velocity profiles (b) Temperature profiles

Figure 12: Two-phase Couette flow: velocity and temperature profiles for EXEX and IMEX schemes.

Velocity, temperature, volume fraction (of fluid 1) and pressure profiles for the IMEX scheme have been plotted in Fig. 13. First and second-order schemes and Glimm's method have been used for the transport step. The results obtained with the anti-diffusive scheme [KL10] for the transport step are not shown here since they were identical to those of Glimm's method. One can see that with Glimm's method, the reference solution is perfectly obtained with only a 100 cells mesh. If the upwind scheme is used in the transport step, Fig. 13 shows that the numerical diffusion of the interface has an impact on the velocity and temperature profiles. A second-order extension of the upwind transport scheme prevents the numerical diffusion of the material interface and there is a better agreement with the unmixed reference solution. The relative error between the numerical pressure computed with the scheme and the pressure reference computed with equation (54) allows a quantitative comparison of the different schemes, see Tab. 3. This comparison shows that the anti-diffusive scheme and Glimm's method are in excellent agreement with the reference solution with only a 100 cells mesh.

Scheme	Relative error (%)
IMEX first-order (Upwind)	7.33
IMEX second-order (Upwind)	4.91
IMEX (anti-diffusive)	0.122
IMEX (GLIMM)	0.160

Table 3: Two-phase Couette flow: relative error on the pressure value for the different schemes.

The fact that the continuous steady solution does not depend on the initial location of the interface between the two fluids is not obvious. Another test case, with an initial condition such as the position of the material interface is close to the steady value, *i.e.* $y_{0,ini} = 0.05$, is therefore designed. To ensure the same initial mass inside the computational domain, the initial densities are given by $\rho_{1,ini} = 50$ kg.m^{-3} and $\rho_{2,ini} = 1.1390$ kg.m^{-3}. One can see in Fig. 14 that the same steady solution is obtained. In addition, with this choice for the initial condition, the interface between the two fluids hardly changes during the transient phase of the simulation. Hence, this initial configuration reduces the duration of the transient phase and thus the numerical diffusion of the interface by the scheme. The choice of the numerical method for the transport step has much less impact on the steady solution: all the profiles in Fig. 14 are very close. This highlights the fact that the numerical steady solution obtained with the upwind scheme depends on the initial position of the material interface.

Finally, the discretization of the dissipative terms in the two-phase flow model has been validated with different test cases. The contribution of neglected terms in predicting the pressure for implicit formulation of the acoustic+dissipative step of the scheme seems to be small. For two-phase flows, the choice of the numerical scheme used in the transport stage

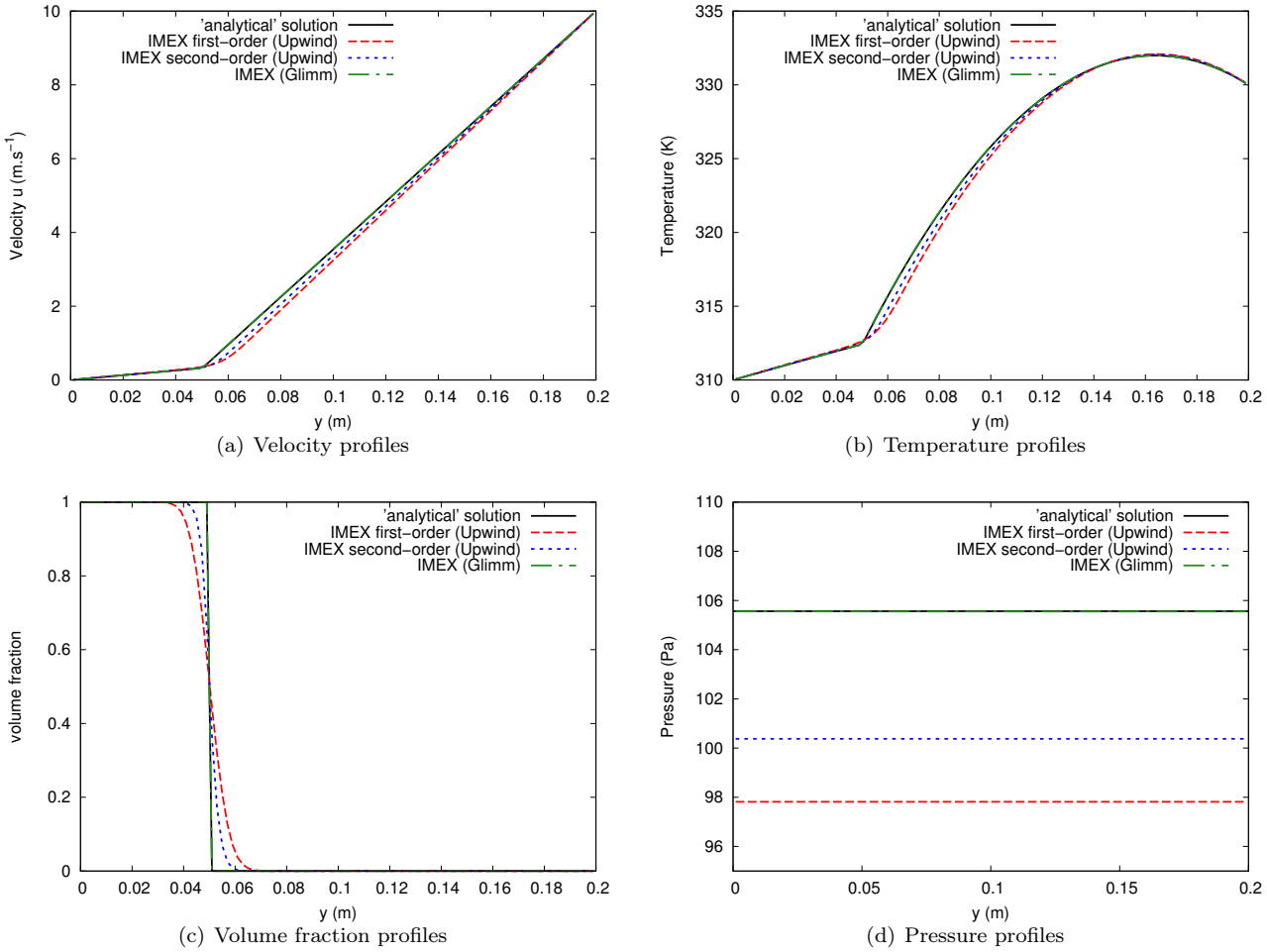

(a) Velocity profiles

(b) Temperature profiles

(c) Volume fraction profiles

(d) Pressure profiles

Figure 13: Two-phase Couette flow: velocity, temperature, volume fraction (of fluid 1) and pressure profiles for the IMEX scheme with first and second-order upwind schemes and Glimm's method for transport step.

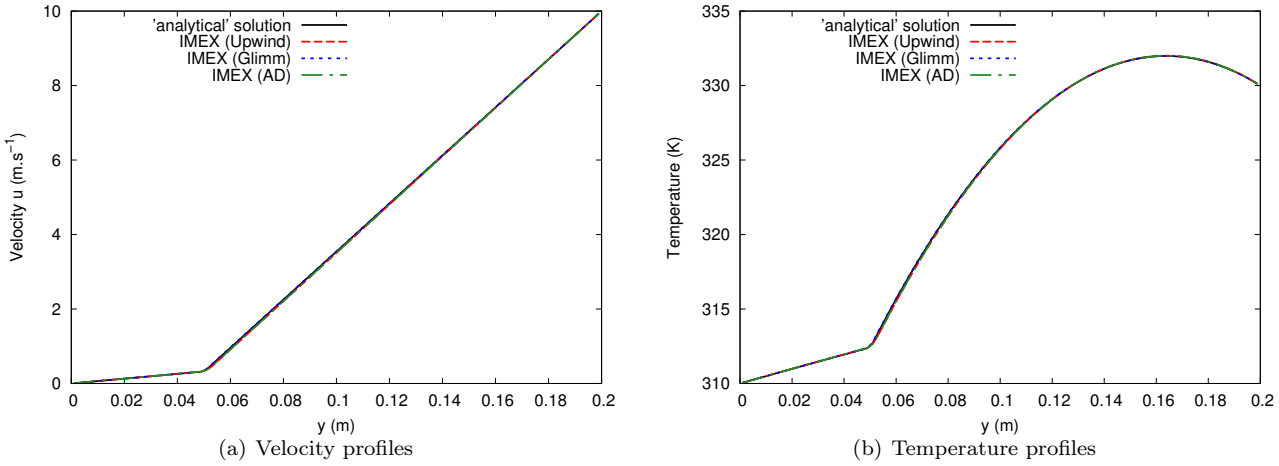

(a) Velocity profiles

(b) Temperature profiles

Figure 14: Two-phase Couette flow: velocity and temperature profiles for the IMEX scheme with first and second-order upwind schemes and Glimm's method for transport step. Initial value of the interface position is close to the steady solution.

plays an important role in the solution. The numerical diffusion generated by the upwind scheme in the transport step is not negligible and has an impact on temperature and velocity profiles. A finer mesh or a second-order scheme can prevent this numerical diffusion and produces a better approximation, closer to the unmixed solution. Numerical schemes limiting the numerical diffusion of the interface between the two fluids in the transport step such as the anti-diffusion scheme [KL10] or Glimm's method [Jun13] will therefore be used in such configurations.

5.4. Numerical simulation of the melting of an aluminium block by an air-filled lid-driven cavity

For the last test case, melting of an aluminium solid block by a lid-driven cavity filled with air is considered. Since the upper wall of the lid-driven cavity is heated, the gas phase induces a significant amount of heat flux by convection to the solid wall. This heat flux leads to the melting of the aluminium solid part and the injection of a liquid phase inside the flow.

In this liquid ablation test case, the initial domain is a rectangle of $[0, 10]$ mm$\times[-10, 10]$ mm separated by the fluid-solid interface at $x_2 = 0$. The fluid region is located in the upper part of the domain, *i.e.* $x_2 > 0$, while the solid block corresponds to the sub-domain characterized by $x_2 < 0$. Side walls of the cavity are considered to be adiabatic. The upper part of the cavity moves from left to right with a lid velocity equal to $u_e = 1$ m.s^{-1}. In order to increase the ablation process, the upper wall is heated to a temperature of 8000 K.

The initial solid temperature is set equal to the aluminium melting temperature, namely $T = 933$ K. To determine the physical data of solid and liquid aluminium, Develay's tables [Dev] which give the numerical values of unalloyed aluminium are used. The density of the solid aluminium near its melting point is $\rho_s = 2550$ kg.m^{-3}. A thermal conductivity $\kappa_s = 208$ W.m^{-1}.K^{-1} and a heat capacity equal to $c_{p,s} = 1240$ J.kg^{-1}.K^{-1} are used in the simulation.

The fluid region is initialized with an air flow assumed to be a perfect gas with $\gamma = 1.4$ at the atmospheric pressure $p = 10^5$ Pa and with an initial density equal to $\rho_g = 0.296$ kg.m^{-3}. Air viscosity is taken equal to $\mu_g = 1.8 \times 10^{-5}$ Pa.s, its thermal conductivity is $\kappa_g = 2\times10^{-2}$ W.m^{-1}.K^{-1} and its heat capacity at constant volume is equal to $c_{v,g} = 905$ J.kg^{-1}.K^{-1}.

For liquid aluminium resulting from the melting of the solid part, the thermal conductivity is set to $\kappa = 90$ W.m^{-1}.K^{-1} [Dev]. Its viscosity is given by $\mu = 1.235 \times 10^{-3}$ Pa.s, while the heat capacity is $c_{v,l} = 970$ J.kg^{-1}.K^{-1}. Its density, for a temperature close to the melting point and atmospheric pressure p_0, is equal to $\rho_l = 2368$ kg.m^{-3}. The enthalpy of fusion for the aluminium is equal to $h_0 = 3.97 \times 10^5$ J.kg^{-1}[Dev]. The liquid phase is modeled by a stiffened-gas equation of state written as

$$p(\rho, \varepsilon) = \Gamma\rho(\varepsilon - q) - (\Gamma + 1)\pi, \tag{55}$$

$$\varepsilon(\rho, T) = q + c_v T + \frac{\pi}{\rho}, \tag{56}$$

where Grüneisen coefficient $\Gamma = \gamma - 1 = 2.14$ and the pressure reference is $\pi = 1.651 \times 10^{10}$ Pa. [Lat13]. The internal energy of reference is $q = h_0 - \frac{p_0}{\rho_0}$.

A 300×300 cells mesh has been used for the numerical simulation. In order to have a reasonable CPU time, 100 processors are used in parallel so that each processor computes a sub-domain of 30×30 cells. With such a mesh, and since solid, liquid and gas phases are present, fully explicit scheme is much too expensive. Indeed, the explicit time step, limited by the diffusion terms, is approximately equal to $\Delta t_{EXEX} \sim 2 \times 10^{-11}$ s. With the implicit-explicit scheme, the time step constraint related to the material velocity is about $\Delta t_{IMEX} \sim 10^{-6}$ s. There is thus a 50 000 ratio between the semi-implicit scheme IMEX and the fully explicit scheme EXEX. The low Mach correction [CGK16] based on a modification of the pressure flux in the acoustic step is used in this numerical simulation to take into account the incompressible nature of the liquid phase. To prevent the numerical diffusion of the interface between the gas phase and the liquid resulting from the melting process, we use the anti-diffusive scheme on the volume fraction [KL10] described in section 3.4.1 for the transport step of the scheme.

The evolution of liquid volume fraction, temperature, and velocity fields as well as mesh deformation for the fluid computational domain at different times are plotted in Figs. 15 and 16.

The air is heated by the top wall and then driven to the right. A recirculation is created in the center of the domain which will allow the gas flow to bring a significant amount of heat flux to the solid part below. The solid is melted by this energy transfer. The liquid phase, represented by the red color on the left column in Figs. 15 and 16, is then injected into the gas flow. The numerical diffusion of the interface between the two fluid phases (liquid and gas) is limited thanks to the anti-diffusion scheme on the volume fraction in the transport step. One can notice that the interface between the liquid

phase and the gas phase in the two-phase flow remains quite horizontal.

The implicit-explicit scheme taking into account the diffusion terms described before seems to be robust enough to compute such configurations involving a two-phase flow with high density ratios between the two phases and a solid part. The implicit treatment of the acoustic+dissipative step and of the numerical scheme used in the solid domain allows larger time step, which are not limited by the dissipative effects. The ALE formulation of the governing equations is also needed since the mesh deformation is following the melting front. Finally, thanks to the parallelization of the code, refined meshes can be used while limiting the impact on the computation time.

6. Conclusion

In order to be able to compute the ablation of metallic thermal protection systems, robust and accurate numerical methods are developed and detailed in this work. In this complex multi-physics problem, the thermal state inside a solid domain needs to be determined and a two-phase viscous flow with a high enthalpy gas and an almost incompressible liquid layer have to be computed. An accurate computation of the melting front is also needed. The governing equations for the two domains and the jumps relations at the interface are described. Since the gas flow and the liquid layer are non-miscible in our application, an extension of five-equation model to dissipative effects is considered. An operator splitting strategy is used to separate the different phenomena according to their own propagation speed in the fluid region. This strategy separates acoustic and dissipative phenomena from the transport one. The hyperbolic part of the acoustic+dissipative step is solved in a non-conservative form using a Godunov-type scheme based on a simple Riemann solver. The Riemann solver slopes are computed using exact positivity conditions for the solution. A classical discretization is used for the dissipative terms, and also for the heat equation inside the solid domain. Since boundary layers have to be accurately computed in order to have a good approximation of the heat flux at the wall, fine meshes are used near the fluid-solid interface. In addition, the acoustic inside the almost incompressible liquid layer is not the main phenomena. Explicit stability conditions are therefore very restrictive for this acoustic+dissipative step. An implicit treatment of the acoustic+dissipative step allows large time steps that are based on the material waves velocity. The numerical fluxes of the hyperbolic part are first computed thanks to an autonomous and linear pressure-velocity sub-system. The specific volume can be directly updated while an iterative process is needed to compute the new internal energy. The transport step is then computed explicitly. Several approaches can be used in order to prevent the numerical diffusion of the material interface between the gas flow and the liquid. The global scheme resulting from the splitting strategy for the five-equation system is conservative. Finally, since moving grids are used to capture accurately the melting front, an ALE formulation of the numerical schemes for both fluid and solid domains is given in a multidimensional framework. A fluid-solid coupling algorithm is then proposed to compute such complex multi-physics problems. Numerical simulations show the validity and the robustness of the IMEX scheme used for the discretization of the five-equation system. The anti-diffusive scheme or Glimm's method needs to be used in the transport step in order to prevent the numerical diffusion of the material interface and to accurately compute the heat flux at the wall. The last test case, namely the melting of an aluminium solid block by a lid-driven cavity filled with air, shows that the numerical tools developed here seem to be robust enough to compute complex configurations involving a two-phase flow with high density ratios and a solid part.

In the future, genuinely two-dimensional schemes to prevent the numerical diffusion of the interface between the gas and the liquid will be considered. This will allow large mesh deformation while limiting the numerical mixture zone. More complex and realistic configurations can be considered with an extension of the splitting strategy to the axisymmetric case. Finally, the treatment of differential ablation of a composite material with a part made of carbon that will sublimate and a metallic part that will melt remains to be studied.

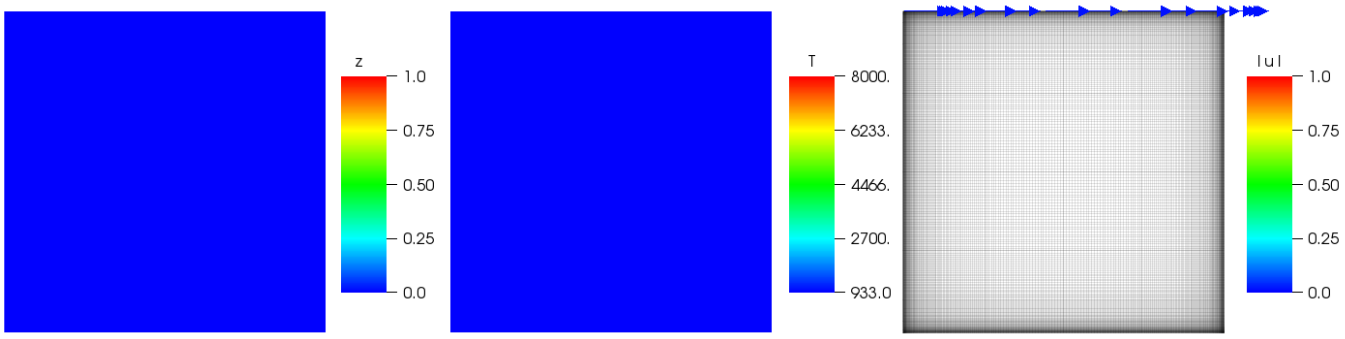

(a) $t = 0$ s

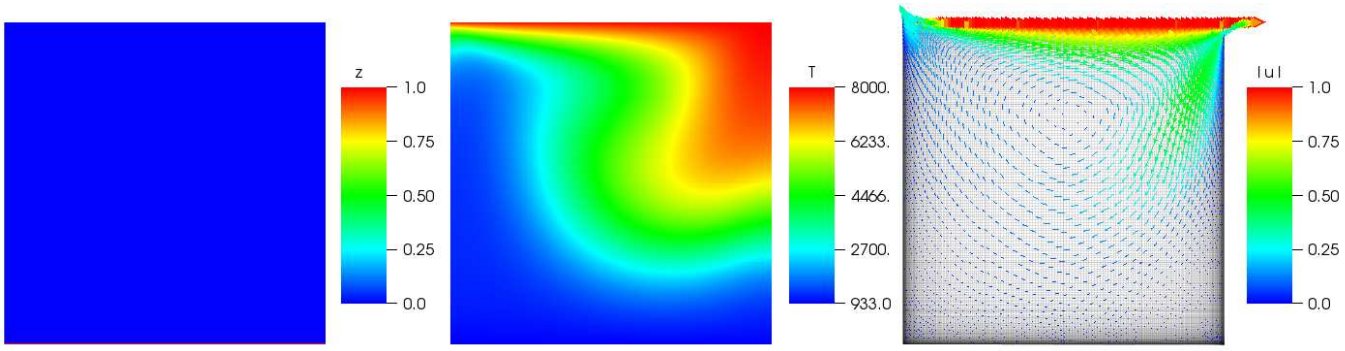

(b) $t = 0.053$ s

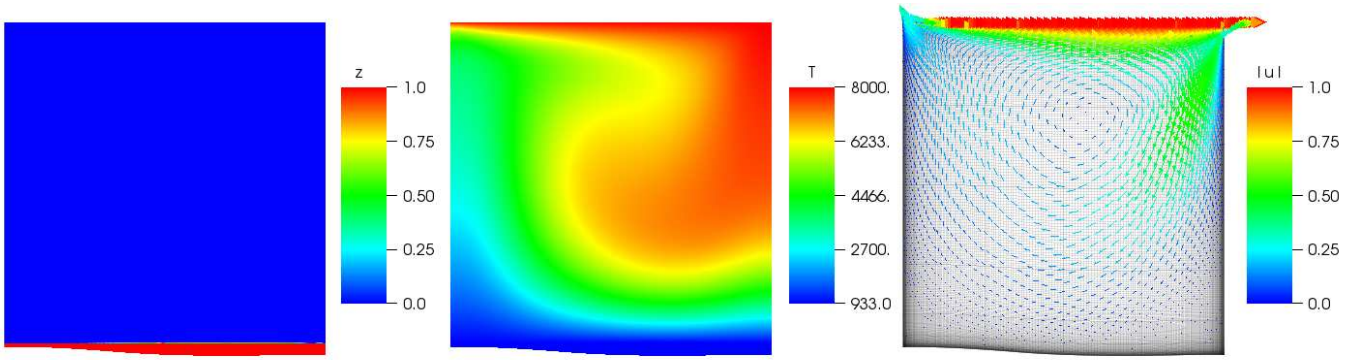

(c) $t = 0.15$ s

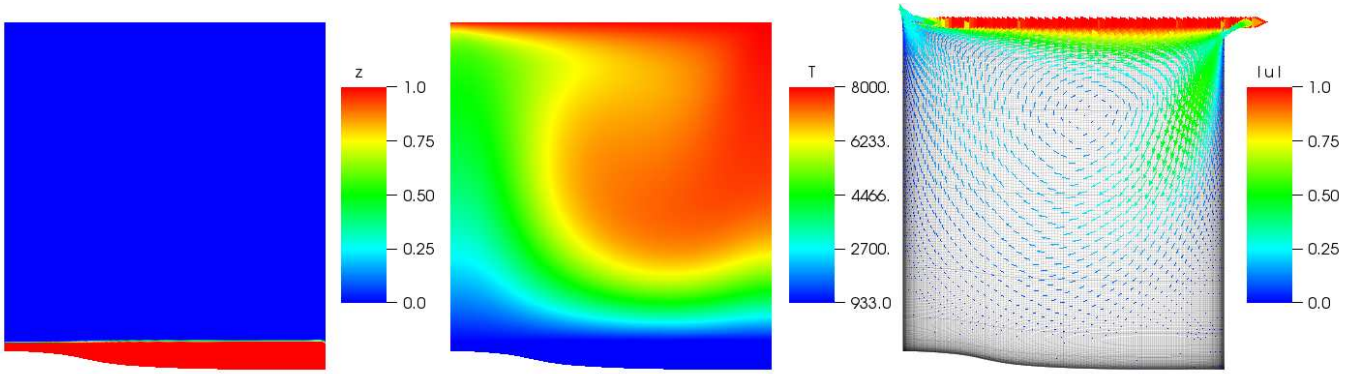

(d) $t = 0.25$ s

Figure 15: Numerical simulation of the melting of an aluminium block by an air-filled lid-driven cavity: evolution of the liquid volume fraction (left), temperature (middle), velocity field and mesh (right) for the fluid computational domain at different times.

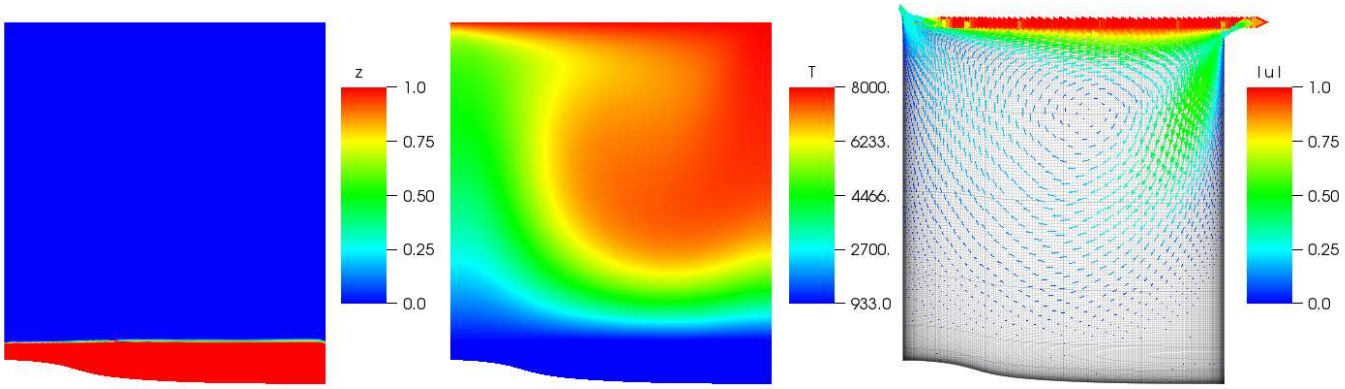

(e) $t = 0.347$ s

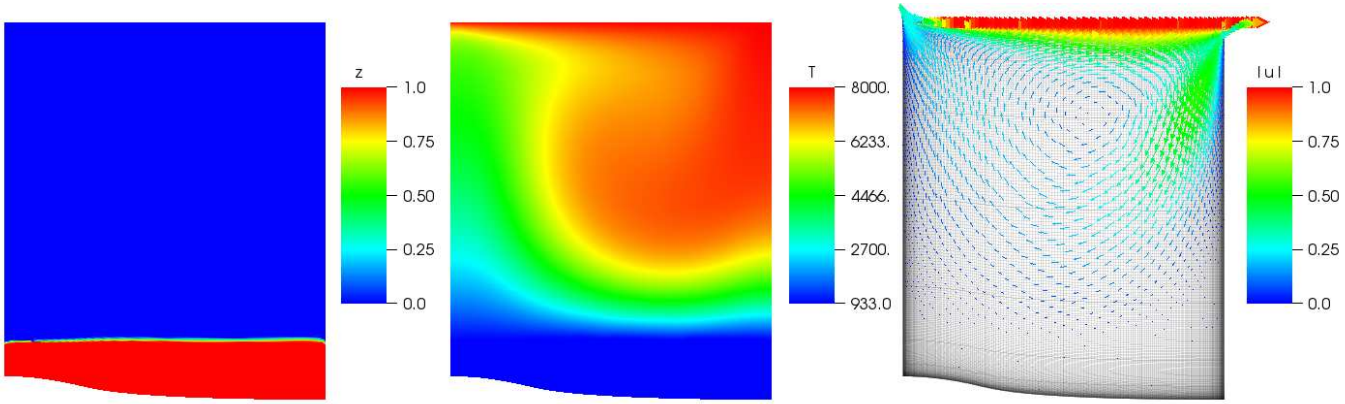

(f) $t = 0.445$ s

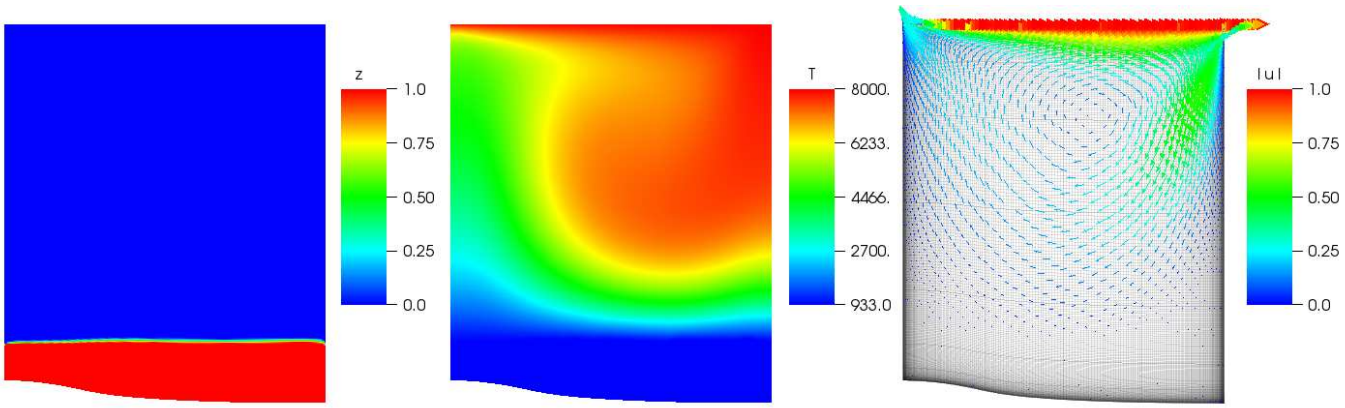

(g) $t = 0.5$ s

Figure 16: Numerical simulation of the melting of an aluminium block by an air-filled lid-driven cavity: evolution of the liquid volume fraction (left), temperature (middle), velocity field and mesh (right) for the fluid computational domain at different times (continued).

Appendix A. Exact solutions of single and two-phase Couette-type flows

In this appendix, exact solutions for plane single and two-phase Couette-type flows are given.

Appendix A.1. Single phase Couette flow

A laminar flow between two horizontal infinite plates is considered. The two surfaces are separated by a distance $y_e - y_w$ The top plate is moving with a constant velocity denoted by u_e, whereas the bottom one is motionless. In addition, the upper plate is heated to the temperature T_e and the lower surface to temperature T_w with $T_e > T_w$. The test-case geometry is described in Fig. 9.

Single phase compressible Navier-Stokes equations reads

$$\begin{cases} \partial_t \rho \quad + \nabla \cdot (\rho \boldsymbol{u}) & = 0, \\ \partial_t (\rho \boldsymbol{u}) + \nabla \cdot (\rho \boldsymbol{u} \otimes \boldsymbol{u}) + \boldsymbol{\nabla} p & = \nabla \cdot \mathsf{T}, \\ \partial_t (\rho E) + \nabla \cdot (\rho E \boldsymbol{u} + p \boldsymbol{u}) & = \nabla \cdot (\mathsf{T} \boldsymbol{u}) - \nabla \cdot \boldsymbol{q}. \end{cases} \tag{A.1}$$

We are looking for a steady solution of this problem. Therefore, all time derivatives of the previous system (A.1) are equal to 0. Since the upper and lower plates are assumed to be infinite, x-derivatives are also equal to 0. Mass conservation equation and boundary conditions reveal that that velocity field is given by $\boldsymbol{u} = (u(y), 0)^T$. The pressure is hence constant inside the entire domain. In this case, the stress tensor reduces to $\mathsf{T} = \begin{pmatrix} 0 & \tau_{xy} \\ \tau_{xy} & 0 \end{pmatrix}$, where $\tau_{xy} = \mu \partial_y u$. The momentum equation is given by

$$\frac{\partial}{\partial y}\left(\mu \frac{\partial u}{\partial y}\right) = 0.$$

In this single phase flow, the viscosity is assumed to be constant in the whole domain. Thus, using boundary conditions $u(y_w) = 0$ and $u(y_e) = u_e$, velocity profile reduces to a linear profile

$$u(y) = u_e \frac{y - y_w}{y_e - y_w}.$$

The energy equation is given by

$$\frac{\partial}{\partial y}\left(\kappa \frac{\partial T}{\partial y}\right) + \mu \left(\frac{\partial u}{\partial y}\right)^2 = 0.$$

Since the thermal conductivity is assumed to be uniform in the fluid, the temperature profile is parabolic. With boundary conditions $T(y_w) = T_w$ and $T(y_e) = T_e$, temperature profile is given by

$$T(y) = T_w + \left(T_e - T_w + \frac{\mu u_e^2}{2\kappa}\left(1 - \frac{y - y_w}{y_e - y_w}\right)\right)\frac{y - y_w}{y_e - y_w}.$$

Global mass conservation can be used in order to find the pressure value $p(y) = P$. Since we have

$$\int_{y_w}^{y_e} \rho(y) \mathrm{d}y = M_{ini},$$

where M_{ini} is the initial mass, then if the fluid equation of state is a stiffened gas, *i.e.* $P = (\gamma - 1)\rho c_v T - \pi$, the pressure value can be deduced

$$P = (\gamma - 1) c_v \left(\int_{y_w}^{y_e} \frac{\mathrm{d}y}{T(y)}\right)^{-1} M_{ini}.$$

Appendix A.2. Two-phase Couette flow

Like in the single-phase case, a physical domain delimited by two infinite horizontal plates separated by a distance $y_e - y_w$ is considered. The upper wall moves at constant speed u_e while the lower wall does not move. In addition, the upper wall is heated to the temperature T_e and the lower wall to the temperature T_w with $T_e > T_w$. For this test case, a two-phase flow

between the two surfaces is considered. The position of the interface between the two fluids is located in $y = y_0$. During the transient phase, the interface between the two fluids will move. The geometry of the test case is described in Fig 11.

We are still looking for a steady solution of this problem and the two plates are assumed to be infinite, therefore all partial derivatives with respect to time and x of the five-equation system (2) are equal to 0. Once again, the pressure field is constant $p(y) = P$ in the entire domain, and velocity field is given by $\boldsymbol{u} = (u(y), 0)^T$. The five-equation system with dissipative terms reduces to

$$\partial_y \left(\mu \partial_y u\right) = 0, \tag{A.2a}$$

$$\mu \left(\partial_y u\right)^2 + \partial_y(\kappa \partial_y T) = 0, \tag{A.2b}$$

with boundary conditions

$$u(y = y_w) = u_w \quad \text{and} \quad u(y = y_e) = u_e,$$
$$T(y = y_w) = T_w \quad \text{and} \quad T(y = y_e) = T_e.$$

Continuity conditions between the two fluids at the interface located in $y = y_0$ require continuity of velocity, shear stress τ_{xy}, temperature and heat flux.

Velocity equation (A.2a) can be integrated in order to find the velocity profile

$$u(y) = \begin{cases} u_0 \dfrac{y - y_w}{L_1} & y_w < y < y_0, \\ u_0 + (u_e - u_0)\dfrac{y - y_0}{L_2} & y_0 < y < y_e, \end{cases} \tag{A.3}$$

where $L_1 = y_0 - y_w$, $L_2 = y_e - y_0$ and u_0 is the velocity at the interface between the two phases. The value of the velocity u_0 is given by shear stress continuity $\tau_{xy} = \mu \partial_y u$ at the interface between the two phases

$$u_0 = \frac{\frac{\mu_2}{L_2} u_e}{\frac{\mu_1}{L_1} + \frac{\mu_2}{L_2}}.$$

Once the velocity profile is found, temperature equation (A.2b) reduces to

$$\partial_y(\kappa \partial_y T) = \begin{cases} -\mu_1 \left(\dfrac{u_0}{L_1}\right)^2 & y_w < y < y_0, \\ -\mu_2 \left(\dfrac{u_e - u_0}{L_2}\right)^2 & y_0 < y < y_e. \end{cases}$$

If again we assume viscosities μ_1 and μ_2 to be constant, then the temperature profile is parabolic in each zone. Using boundary conditions, we find

$$T(y) = \begin{cases} -\dfrac{\mu_1 u_0^2}{2\kappa_1} \left(\dfrac{y - y_w}{L_1}\right)^2 + \left(T_0 - T_w + \dfrac{\mu_1 u_0^2}{2\kappa_1}\right) \dfrac{y - y_w}{L_1} + T_w & y_w < y < y_0, \\ -\dfrac{\mu_2 \left(u_e - u_0\right)^2}{2\kappa_2} \left(\dfrac{y - y_0}{L_2}\right)^2 + \left(T_e - T_0 + \dfrac{\mu_2 \left(u_e - u_0\right)^2}{2\kappa_2}\right) \dfrac{y - y_0}{L_2} + T_0 & y_0 < y < y_e, \end{cases} \tag{A.4}$$

where T_0 is the temperature at the interface between the two phases. This temperature can be obtained thanks to the heat flux continuity at $y = y_0$

$$T_0 = \frac{1}{\frac{\kappa_1}{L_1} + \frac{\kappa_2}{L_2}} \left(\frac{\kappa_1}{L_1} T_w + \frac{\kappa_2}{L_2} T_e + \frac{\mu_1 u_0^2}{2L_1} + \frac{\mu_2 \left(u_e - u_0\right)^2}{2L_2}\right).$$

The location y_0 of the interface between the two fluids and the pressure at the steady state are still unknown. To do this, global mass conservation can be used

$$\int_{y_w}^{y_e} \rho(y)\mathrm{d}y = M_{ini},$$

where M_{ini} is the initial mass. In case where both fluids are stiffened gases, mass conservation reads

$$\frac{P+\pi_1}{(\gamma_1-1)c_{v_1}}\int_{y_w}^{y_0}\frac{\mathrm{d}y}{T(y)} + \frac{P+\pi_2}{(\gamma_2-1)c_{v_2}}\int_{y_0}^{y_e}\frac{\mathrm{d}y}{T(y)} = M_{ini}.$$

Temperature profile have been shown to be of the form of $T(y) = ay^2 + by + c$ in each zone. Those terms can be integrated to get

$$I = \int_{y_1}^{y_2}\frac{\mathrm{d}y}{ay^2+by+c} = \frac{1}{a(r_1-r_2)}\ln\left(\frac{(y_2-r_1)(y_1-r_2)}{(y_1-r_1)(y_2-r_2)}\right).$$

with $\Delta = b^2 - 4ac > 0$ and $r_1 < y_1 < y_2 < r_2$ where $r_1 = \min\left(\frac{-b\pm\sqrt{\Delta}}{2a}\right)$ and $r_2 = \max\left(\frac{-b\pm\sqrt{\Delta}}{2a}\right)$.
The pressure can be determined from the interface position y_0. Let us denote by $I_1 = \int_{y_w}^{y_0}\frac{\mathrm{d}y}{T(y)}$ and $I_2 = \int_{y_0}^{y_e}\frac{\mathrm{d}y}{T(y)}$ integral of the inverse of the temperature in the two regions. One finally gets

$$P = \frac{M_{ini} - \frac{\pi_1 I_1}{(\gamma_1-1)c_{v_1}} - \frac{\pi_2 I_2}{(\gamma_2-1)c_{v_2}}}{\frac{I_1}{(\gamma_1-1)c_{v_1}} + \frac{I_2}{(\gamma_2-1)c_{v_2}}}. \tag{A.5}$$

In the case of a two-phase Couette flow, velocity (A.3) and temperature (A.4) profiles and the value of the pressure P (A.5) are given as functions of the position of the fluid interface y_0. However, another equation is needed to be able to fully determine the steady state. Global energy conservation equation cannot be used since temperatures are enforced on the walls of the domain. Nonetheless, since there is no mass transfer between the two fluid phase, the mass of each fluid phase is also constant. The mass conservation for the first fluid phase reads

$$\int_{y_w}^{y_0} \rho(y)\mathrm{d}y = M^1_{ini},$$

where M^1_{ini} is the initial mass of the first fluid phase. Once again, with a stiffened gas, one can find

$$(P(y_0)+\pi_1)I_1(y_0) = M^1_{ini}(\gamma_1-1)c_{v_1}.$$

The position of the material interface y_0 can be determined by solving this non-linear equation. The steady solution of this two-phase Couette flow is then completely defined.

References

[ACK02] G. Allaire, S. Clerc, and S. Kokh. A five-equation model for the simulation of interfaces between compressible fluids. *J. Comput. Phys.*, 181:577–616, 2002.

[AS07] H. T. Ahn and M. Shashkov. Multi-material interface reconstruction on generalized polyhedral meshes. *J. Comput. Phys.*, 226(2):2096–2132, 2007.

[BDJP19] P. Bruel, S. Delmas, J. Jung, and V. Perrier. A low Mach correction able to deal with low Mach acoustics. *J. Comput. Phys.*, 378:723–759, 2019.

[BHJ+13] M. Bachmann, P. Helluy, J. Jung, H. Mathis, and S. Müller. Random sampling remap for compressible two-phase flows. *Comput. Fluids*, 86:275–283, 2013.

[BHMS13] J. Breil, T. Harribey, P.-H. Maire, and M. Shashkov. A multi-material ReALE method with MOF interface reconstruction. *Comput. Fluids*, 83:115–125, 2013.

[BL15] X. Blanc and E. Labourasse. A positive scheme for diffusion problems on deformed meshes. *ZAMM Zeitschrift fur Angew. Math. und Mech.*, 2015.

[BN86] M.R. Baer and J.W. Nunziato. A two-phase mixture theory for the deflagration-to-detonation transition (DDT) in reactive granular materials. *Int. J. Multiphase Flow*, 12(6):861–889, 1986.

[BN09] B. Braconnier and B. Nkonga. An all-speed relaxation scheme for interface flows with surface tension. *J. Comput. Phys.*, 228:5722–5739, 2009.

[BNM10] D. Bianchi, F. Nasuti, and E. Martelli. Navier-Stokes simulations of hypersonic flows with coupled graphite ablation. *J. Spacecraft Rockets*, 47(4):554–562, 2010.

[Bou04] F. Bouchut. *Nonlinear stability of finite Volume Methods for hyperbolic conservation laws: And Well-Balanced schemes for sources*. Springer Science & Business Media, 2004.

[CDK12] F. Cordier, P. Degond, and A. Kumbaro. An Asymptotic-Preserving all-speed scheme for the Euler and Navier–Stokes equations. *J. Comput. Phys.*, 231(17):5685–5704, 2012.

[CGK16] C. Chalons, M. Girardin, and S. Kokh. An all-regime Lagrange-Projection like scheme for the gas dynamics equations on unstructured meshes. *Comm. Comput. Phys.*, 20(1):188–233, 006 2016.

[CGK17] C. Chalons, M. Girardin, and S. Kokh. An all-regime Lagrange-Projection like scheme for 2D homogeneous models for two-phase flows on unstructured meshes. *J. Comput. Phys.*, 335:885–904, 2017.

[Cha04] G. Chanteperdrix. *Modélisation et simulation numérique d'écoulements diphasiques à surface libre. Application à l'étude des mouvements de liquides dans les réservoirs de véhicules spatiaux*. PhD thesis, Ecole Nationale Supérieure de l'Aéronautique et de l'Espace, 2004.

[CNPT10] F. Coquel, Q. Nguyen, M. Postel, and Q. Tran. Entropy-satisfying relaxation method with large time-steps for Euler IBVPs. *Mathematics of Computation*, 79(271):1493–1533, 2010.

[Col82] P. Colella. Glimm's method for gas dynamics. *SIAM J. Sci. Statist. Comput.*, 3(1):76–110, 1982.

[Del10] S. Dellacherie. Analysis of Godunov type schemes applied to the compressible Euler system at low Mach number. *J. Comput. Phys.*, 229:978–1016, 2010.

[Dev] R. Develay. Données numériques sur l'aluminium non allié. Techniques de l'ingénieur, traité Matériaux métalliques. Formulaire.

[DJOR16] S. Dellacherie, J. Jung, P. Omnes, and P.-A. Raviart. Construction of modified Godunov-type schemes accurate at any Mach number for the compressible Euler system. *Math. Models Methods Appl. Sci.*, 26(13):2525–2615, 2016.

[DJY07] P. Degond, S. Jin, and J. Yuming. Mach-number uniform asymptotic-preserving gauge schemes for compressible flows. *Bulletin of the Institute of Mathematics, Academia Sinica*, 2(4):851, 2007.

[DKL16] B. Després, S. Kokh, and F. Lagoutière. Sharpening methods for finite volume schemes. *Handb. Numer. Anal.*, 17:77–102, 2016.

[DL99] B. Després and F. Lagoutière. Un schéma non linéaire anti-dissipatif pour l'équation d'advection linéaire. *C. R. Acad. Sci. Paris, Série I*, 328(10):939–943, 1999.

[DLL07] B. Després, E. Labourasse, and F. Lagoutière. The Vofire method for multicomponent flows on unstructured meshes. *Jacques-Louis Lions Report R07052*, 2007.

[DS08] V. Dyadechko and M. Shashkov. Reconstruction of multi-material interfaces from moment data. *J. Comput. Phys.*, 227(11):5361–5384, 2008.

[EDKT17] M.F.P. ten Eikelder, F. Daude, B. Koren, and A.S. Tijsseling. An acoustic-convective splitting-based approach for the Kapila two-phase flow model. *J. Comput. Phys.*, 331(1):188–208, 2017.

[FBC+11] M. Billaud Friess, B. Boutin, F. Caetano, G. Faccanoni, S. Kokh, F. Lagoutière, and L. Navoret. A second order anti-diffusive Lagrange-remap scheme for two-component flows. In *ESAIM: Proceedings*, volume 32, pages 149–162. EDP Sciences, 2011.

[FK13] V. Faucher and S. Kokh. Extended Vofire algorithm for fast transient fluid–structure dynamics with liquid–gas flows and interfaces. *J. Fluids Struct.*, 39:102–125, 2013.

[FK14] M. Billaud Friess and S. Kokh. Simulation of sharp interface multi-material flows involving an arbitrary number of components through an extended five-equation model. *J. Comput. Phys.*, 273:488–519, 2014.

[FL11] T. Flåtten and H. Lund. Relaxation two-phase flow models and the subcharacteristic condition. *Mathematical Models and Methods in Applied Sciences*, 21(12):2379–2407, 2011.

[Gal00] G. Gallice. Schémas de type Godunov entropiques et positifs préservant les discontinuités de contact. *C. R. Acad. Sci. Paris, Série I*, 331(2):149–152, 2000.

[Gal03] G. Gallice. Positive and entropy stable Godunov-type schemes for gas dynamics and MHD equations in Lagrangian or Eulerian coordinates. *Numer. Math.*, 94:673–713, 2003.

[Gli65] J. Glimm. Solutions in the large for nonlinear hyperbolic systems of equations. *Comm. Pure Appl. Math.*, 18(4):697–715, 1965.

[GM04] H. Guillard and A. Murrone. On the behavior of upwind schemes in the low Mach number limit: II. Godunov type schemes. *Comput. Fluids*, 33(4):655–675, 2004.

[GR91] E. Godlevski and P.-A. Raviart. *Hyperbolic systems of conservation laws.* Mathématiques et Applications, Ellipses, Paris, 1991.

[GV99] H. Guillard and C. Viozat. On the behaviour of upwind schemes in the low Mach number limit. *Comput. Fluids*, 28(1):63–86, 1999.

[HJ13] P. Helluy and J. Jung. OpenCL numerical simulations of two-fluid compressible flows with a 2D random choice method. *International J. Finite Volumes*, 10:1–38, 2013.

[HJL12] J. Haack, S. Jin, and J. Liu. An all-speed asymptotic-preserving method for the isentropic Euler and Navier-Stokes equations. *Comm. Comput. Phys.*, 12(04):955–980, 2012.

[HN81] C. W. Hirt and B. D. Nichols. Volume of fluid (VOF) method for the dynamics of free boundaries. *J. Comput. Phys.*, 39(1):201–225, 1981.

[HSD+19] D. Henneaux, P. Schrooyen, B. Dias, A. Turchi, P. Chatelain, and T. Magin. Towards a high-fidelity multiphase solver with application to space debris aerothermal ablation modeling. In *AIAA Aviation 2019 Forum*, page 2876, 2019.

[Jun13] J. Jung. *Schémas numériques adaptés aux accélérateurs multicœurs pour les écoulements bifluide*. PhD thesis, Université de Strasbourg, 2013.

[KL10] S. Kokh and F. Lagoutière. An anti-diffusive numerical scheme for the simulation of interfaces between compressible fluids by means of five-equation model. *J. Comput. Phys.*, 229:2773–2809, 2010.

[KMB+01] A.K. Kapila, R. Menikoff, J.B. Bdzil, S.F. Son, and D. S. Stewart. Two-phase modeling of deflagration-to-detonation transition in granular materials: Reduced equations. *Physics of Fluids (1994-present)*, 13(10):3002–3024, 2001.

[Lag00] F. Lagoutière. *Modélisation mathématique et résolution numérique de problèmes de fluides compressibles à plusieurs constituants*. PhD thesis, Université Pierre-et-Marie-Curie (Paris 6), 2000.

[Lat13] M. Latige. *Simulation numérique de l'ablation liquide*. PhD thesis, Université Sciences et Technologies-Bordeaux I, 2013.

[LF96] M. Lesoinne and C. Farhat. Geometric conservation laws for flow problems with moving boundaries and deformable meshes, and their impact on aeroelastic computations. *Comput. Methods Appl. Mech. Engrg.*, 134(1-2):71–90, 1996.

[LMNS13] S. Le Martelot, B. Nkonga, and R. Saurel. Liquid and liquid–gas flows at all speeds. *J. Comput. Phys.*, 255:53–82, 2013.

[LMSN14] S. Le Martelot, R. Saurel, and B. Nkonga. Towards the direct numerical simulation of nucleate boiling flows. *Int. J. Multiphase Flow*, 66:62–78, 2014.

[LP09] C. Le Potier. A nonlinear finite volume scheme satisfying maximum and minimum principles for diffusion operators. *Int. J. Finite Volumes*, pages 1–20, 2009.

[MB14] A. Martin and I. D. Boyd. Strongly coupled computation of material response and nonequilibrium flow for hypersonic ablation. *J. Spacecraft Rockets*, 52(1):89–104, 2014.

[MC13] F. S. Milos and Y.-K. Chen. Ablation, thermal response, and chemistry program for analysis of thermal protection systems. *J. Spacecraft Rockets*, 50(1):137–149, 2013.

[MG05] A. Murrone and H. Guillard. A five equation reduced model for compressible two phase flow problems. *J. Comput. Phys.*, 202(2):664 – 698, 2005.

[MG08] A. Murrone and H. Guillard. Behavior of upwind scheme in the low Mach number limit: III. preconditioned dissipation for a five equation two phase model. *Comput. Fluids*, 37(10):1209–1224, 2008.

[MSNA02] J. Massoni, R. Saurel, B. Nkonga, and R. Abgrall. Proposition de méthodes et modèles Eulériens pour les problèmes à interfaces entre fluides compressibles en présence de transfert de chaleur: Some models and Eulerian methods for interface problems between compressible fluids with heat transfer. *Int. J. Heat Mass Transfer*, 45(6):1287–1307, 2002.

[Mul10] N. J. Mullenix. *Fully Coupled Model for High-Temperature Ablation and a Reative-Riemann Solver for its Solution.* PhD thesis, University of Akron, 2010.

[NW76] W. F. Noh and P. Woodward. SLIC (Simple Line Interface Calculation). In *Proceedings of the Fifth International Conference on Numerical Methods in Fluid Dynamics June 28–July 2, 1976 Twente University, Enschede*, pages 330–340. Springer, 1976.

[OS88] S. Osher and J. A. Sethian. Fronts propagating with curvature-dependent speed: algorithms based on Hamilton-Jacobi formulations. *J. Comput. Phys.*, 79(1):12–49, 1988.

[PGM17] S. Peluchon, G. Gallice, and L. Mieussens. A robust implicit–explicit acoustic-transport splitting scheme for two-phase flows. *J. Comput. Phys.*, 339:328–355, 2017.

[PS14] M. Pelanti and K.-M. Shyue. A mixture-energy-consistent six-equation two-phase numerical model for fluids with interfaces, cavitation and evaporation waves. *J. Comput. Phys.*, 259:331 – 357, 2014.

[Rie11] F. Rieper. A low-Mach number fix for Roe's approximate Riemann solver. *J. Comput. Phys.*, 230(13):5263–5287, 2011.

[SA99] R. Saurel and R. Abgrall. A simple method for compressible multifluid flows. *SIAM J. Sci. Comput.*, 21 (3):1115–1145, 1999.

[SPB09] R. Saurel, F. Petitpas, and R. A. Berry. Simple and efficient relaxation methods for interfaces separating compressible fluids, cavitating flows and shocks in multiphase mixtures. *J. Comput. Phys.*, 228(5):1678 – 1712, 2009.

[Ste91] J. Stefan. Uber die theorie der eisbildung, insbesondere ueber die eibildung im polar -meere. *Ann. Phys. Chem.*, 42:269–286, 1891.

[SW84] H. B. Stewart and B. Wendroff. Two-phase flow: Models and methods. *J. Comput. Phys.*, 56(3):363 – 409, 1984.

[TMD+08] B. Thornber, A. Mosedale, D. Drikakis, D. Youngs, and R.J.R. Williams. An improved reconstruction method for compressible flows with low Mach number features. *J. Comput. Phys.*, 227(10):4873 – 4894, 2008.

[Tor97] E.F. Toro. *Riemann solvers and Numerical Methods for Fluid Dynamics.* Springer, 1997.

[Tur87] E. Turkel. Preconditioned methods for solving the incompressible and low speed compressible equations. *J. Comput. Phys.*, 72(2):277–298, 1987.

[Wu17] J. Wu. Vertex-centered linearity-preserving schemes for nonlinear parabolic problems on polygonal grids. *J. Sci. Comput.*, 71(2):499–524, 2017.

[ZSW17] X. Zhang, S. Su, and J. Wu. A vertex-centered and positivity-preserving scheme for anisotropic diffusion problems on arbitrary polygonal grids. *J. Comput. Phys.*, 2017.